NASA TECHNICAL NOTE

NASA TN D-3656

NASA TN D-3656

HIGH-ENERGY ION BEAMS USED TO ACCELERATE HYDROGEN PROPELLANT ALONG MAGNETIC TUBE OR FLUX

by Gerald W. Englert

Lewis Research Center
Cleveland, Ohio

NATIONAL AERONAUTICS AND SPACE ADMINISTRATION • WASHINGTON, D. C. • OCTOBER 1966

NASA TN D-3656

HIGH-ENERGY ION BEAMS USED TO ACCELERATE HYDROGEN PROPELLANT ALONG MAGNETIC TUBE OF FLUX

By Gerald W. Englert

Lewis Research Center
Cleveland, Ohio

NATIONAL AERONAUTICS AND SPACE ADMINISTRATION

For sale by the Clearinghouse for Federal Scientific and Technical Information
Springfield, Virginia 22151 – Price $2.00

HIGH-ENERGY ION BEAMS USED TO ACCELERATE HYDROGEN PROPELLANT ALONG MAGNETIC TUBE OF FLUX

by Gerald W. Englert

Lewis Research Center

SUMMARY

An analytical study was made of the transfer of energy from a high-intensity beam of light-weight ions to a hydrogen target. The hydrogen was confined to a region bounded by a magnetic tube of flux. Under certain conditions the gradient of the magnetic field was quite effective in accelerating sizable mass flows of hydrogen which resulted in large increases of momentum over that of the impinging beam. Interaction between the various species of particles was studied in detail.

The analysis was applied to the efflux of ions from a hypothetical 100-megawatt thermonuclear reactor. The stream of ions escaping from the weaker mirror of a magnetic mirror system was represented by a high-flux-density monoenergetic unidirectional beam. Hydrogen was admitted into this beam slightly downstream of the weak mirror exit station. Thus, the hydrogen served as the propellant and the reactor as the energy source of a thermonuclear rocket.

A range of magnet sizes and strengths, energy and cross-sectional areas of the beam, and hydrogen flow rates were studied. Energy transfer was most effective when the beam was concentrated on a dense closely confined target. Ionization and acceleration of the hydrogen was usually quite rapid near the station where the beam first impinged on the target. Beyond a distance of about one magnet diameter downstream of this station, the velocity was increased and density decreased to values that permitted little further energy transfer. The fractional ionization then stayed essentially constant; however, acceleration continued for another two magnet diameters because of the continuing high gradient of the magnetic field that interacted with the remaining thermal energy in the propellant electrons.

At low hydrogen flow rates only a small amount of energy could be transferred from the beam to the target. At high flow rates, loss was mainly due to power consumed in ionizing the hydrogen. The momentum (thrust) of the hydrogen could be increased to seven times that of the beam with an overall energy transfer efficiency of 25 percent.

INTRODUCTION

Numerous theoretical and experimental stopping-power studies (refs. 1 to 4) were made wherein an ion beam impinges upon and transfers its energy to a gaseous target. In the present study the target is confined to a slender region bounded by an axisymmetric tube of magnetic field lines. The flux tube is concentric with the axis of the magnetic field coil. Such a flux tube can form a type of "magnetic nozzle" as energy gained by the target gas is in part converted into a directed translational mode along diverging field lines. The gas initially requires a confining wall. Where required, the wall is congruent with the field lines. However, the gas that is ionized later can be magnetically confined. A net increase of momentum, or thrust, over that of the impinging beam alone could result as the additional mass of target material (propellant) is accelerated. This report investigates the conditions under which such results can be theoretically realized.

Application is made to a conceptual thermonuclear rocket, the basic constituent of which is a reaction volume confined by a magnetic mirror system having one mirror slightly weaker than the other (fig. 1). A stream of high-energy helium 3 and deuterium ions is emitted from the weaker mirror (refs. 5 to 7) providing a small amount of thrust at a very high specific impulse. For interplanetary propulsion the thrust of such a system must be greatly increased by the addition of much more propellant (ref. 8). Hydrogen is used as the additional propellant and is accelerated by interaction with the emerging reactor ions and the magnetic field of the local mirror. The hydrogen has previously been used to cool a high-temperature shield about the reactor (fig. 1) and is in a dissociated or monatomic state. The present analysis approximates the efflux of reactor particles from the weaker mirror by a monoenergetic unidirectional beam. (The mks system of units is used unless otherwise specified.)

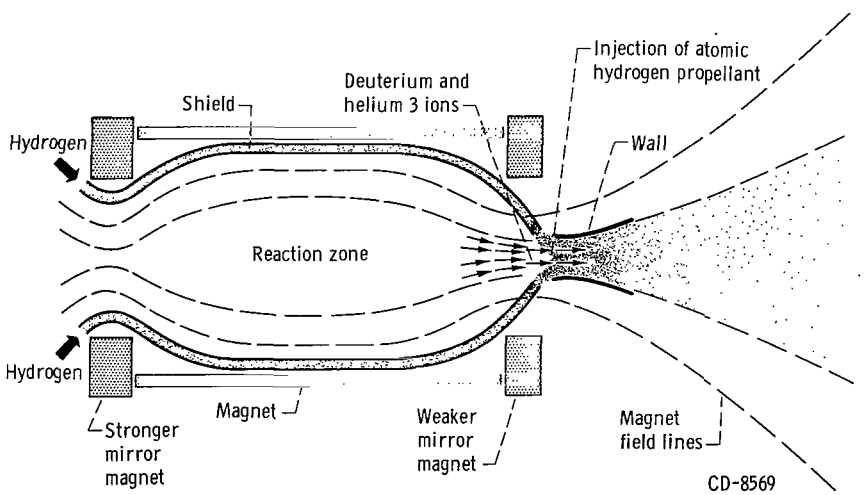

Figure 1. - Schematic of basic thermonuclear rocket configuration.

ANALYSIS

The analysis is based primarily on the theory of classical particles. In general the ensemble of particles considered consists of electrons, ions, and neutral atoms. Particles initially in the beam include electrons plus one or more species of ions. The propellant, or target, is initially in the form of monatomic hydrogen, some of which is soon ionized to form two additional species - electrons and protons.

The behavior of the propellant species was studied as usual by conservation equations of mass, momentum, and energy. Beam particles, however, were considered influential in this study only as a source of energy. Preliminary calculations indicated that in the range of interest for propulsion the density and flow rates of propellant particles are much greater than those of the beam particles and that only the propellant species are of any consequence in the mass and momentum balances. The energy of the beam species and the density, velocity, and temperature of the propellant are determined as functions of distance along the magnetic field lines. The study is limited to a one-dimensional analysis in which the flow properties are uniform across any surface normal to the flow direction.

Transfer of Energy from Beam Particles

Beam composition. - The energy is assumed to be initially in the form of a high-intensity monoenergetic unidirectional beam of charged particles flowing along magnetic field lines. Such a beam undergoes a certain fractional neutralization because of charge exchange when it impinges on a neutral target gas (ref. 9). Very little momentum transfer occurs during a charge exchange event, and, thus, very little change in directions is expected for the incident particles. Thus, if the charged particles initially impinge upon the propellant as a unidirectional beam, they should remain so even if neutralized. Each atomic species of the beam is assumed to be monoenergetic at any given axial station in the magnetic flux tube. This assumption is consistent with the data of reference 10, which show that there is very little spread of energy about an average as a beam of ions transfers its energy to a plasma.

Impingement of charged particles on a neutral target has been studied experimentally by many investigators. In these experiments the bombardment chamber was large or attached to an abundant reservoir of target material. The beam thus underwent a change in charge composition whereas the target material, for all practical purposes, remained the same. Herein, however, the target boundary is the same as that of the beam and also the flow of target material is limited. The target can thus undergo sizable changes in charge composition.

If the target material has a low density (within a certain range) enough collisions occur to permit the beam to come to an equilibrium composition; yet the collisions are few enough that the energy of the beam is not appreciably degraded (refs. 4 and 9). After equilibrium is reached the beam composition is essentially independent of the distance that the beam travels. Experiments conducted under these conditions are useful for studying charge exchange and ionization cross sections as functions of beam energy. Herein, however, the target is often dense enough that the beam energy is constantly degrading along its path of travel. Thus, both beam and target have equilibrium compositions, which, among other things, are functions of distance in the direction of beam travel. Consider, for example, a beam that is initially composed of doubly charged helium 3 ions, singly charged deuterium ions, and electrons (see APPLICATION section and appendix B). Shortly after impingement on an atomic hydrogen target the beam is composed of doubly and singly charged helium 3 ions, singly charged deuterium ions, helium 3 and deuterium neutrals, and electrons; whereas, the target is composed of protons, electrons, and neutral hydrogen atoms. The fractions of the various species depend on the energies transferred and thus on the distance inside the target. A detailed study of this phenomenon would necessitate the inclusion of approximately 25 interactions in an already complex problem.

The problem is made somewhat more manageable by restricting the analysis to beams which are composed predominantly of neutrals and singly charged ions. Hydrogen and its isotopes obviously fall into this category. Helium can also be included if the beam energy is kept below 100 keV because the probability of a doubly charged helium particle obtaining an electron from a target hydrogen atom far outweighs (by more than a factor of 10) any of the other charge-exchange probabilities for this energy range (ref. 9).

Stopping power. - The energy exchange per unit distance per incident particle dE_R/dx is often written as the number density of the target material n_t times the total stopping power $(1/n_t)(dE_R/dx)$. The total stopping power can be expressed as the weighted sum of the partial stopping powers of each of the charge species plus the energy loss due to collisions involving charge exchange (refs. 3 and 4). Thus, for this restricted analysis

$$\frac{1}{n_t}\frac{dE_R}{dx} = F_{R^0}\frac{1}{n_t}\frac{dE_{R^0}}{dx} + F_{R^+}\frac{1}{n_t}\frac{dE_{R^+}}{dx} + \text{Loss due to charge exchange}$$

where F_{R^0} and F_{R^+} are the equilibrium fractions of neutral and singly charged ions in the beam, respectively.

A conclusion reached in reference 1 is that the partial stopping powers for both neutral and singly charged hydrogen atoms are close to the same magnitude. With this premise and neglecting energy loss due to charge exchange, total stopping power was

closely approximated by

$$\frac{1}{n_t}\frac{dE_H}{dx} \approx \left(F_{H^+} + F_{H^0}\right)\frac{1}{n_t}\frac{dE_{H^+}}{dx} = \frac{1}{n_t}\frac{dE_{H^+}}{dx}$$

This procedure also approximates reasonably well the total stopping power for helium in the energy range below 100 keV (see appendix C).

Analytical stopping power expressions are reviewed in references 11 and 12. All the expressions are of the form

$$\frac{1}{n_t}\frac{dE_R}{dx} \approx (\text{constant})\left(\frac{(z_t z_R)^2 \frac{m_R}{m_t}}{E_R}\right)\left(\text{slowly varying function of } \frac{v_t}{v_R}\right)$$

where the subscripts t and R denote target particles and incident particles, respectively. The m_R/m_t term shows that the relatively heavy nuclei of the target particles receive very little energy in comparison with that received by the target electrons.

The stopping power expressions also show that a beam of incident electrons having energies of the same magnitude as the incident ions would give a relatively insignificant amount of energy to the target. On the other hand, if the beam electrons were at an energy so much lower than that of the ions that the energy transfer rate from them was significant, then their energy content would be so low that only a negligible total amount of energy would be available from them. Thus, the electrons in the beam were assumed to serve only as producers of a neutral net flux of charge of the beam species (this will be discussed further in the APPLICATION section).

Stopping power for species closely related to the one of interest herein has been determined experimentally (refs. 3 and 4). The theory of reference 2 gives satisfactory agreement with these measurements; therefore, it was applied to the singly charged ions impinging on neutral hydrogen atoms in appendix C. From equation (C3)

$$\frac{dE_R}{dx} = -\frac{n_n e^4 \frac{m_R}{m_e}}{16\pi\epsilon^2 E_R\left(1 + w_R^2\right)^{3/2}} \begin{cases} 2 \ln \frac{2}{w_R} + \frac{8}{3} & \text{when } U \le KE_R(1 - w_R) \\ \ln \frac{4.825}{w_R} + 1.804 + \frac{0.833}{w_R} - \frac{w_R}{6} - \frac{w_R^3}{96} & \text{when } U \ge KE_R(1 - w_R) \end{cases} \quad (1)$$

where

$$w_R = \sqrt{\frac{m_R}{m_e}\frac{E_e}{E_R}} = \frac{v_e}{v_R}$$

$$K = \frac{4m_e m_R}{(m_e + m_R)^2}$$

the quantities E_R and m_R are the energy and mass of a single-incident or impinging-reactor particle, and n_n, E_e, and m_e are the number density, energy, and mass of the target material which are the ground state electrons of the hydrogen atoms, respectively. Equation (1) is based on the fact that for hydrogen atoms, the kinetic energy E_e is equal to the ionization potential U.

An appreciable amount of energy can also be transferred to the free electrons that are formed as the propellant is ionized. An expression to determine the amount of this energy exchange is derived in appendix C by use of the kinetic theory of reference 13. From equation (C4)

$$\frac{dE_R}{dx} = -\frac{n_e e^4 F_{R^+} \frac{m_R}{m_e}}{8\sqrt{2\pi}\,\pi\epsilon^2 E_R \left(1 + \frac{m_R kT_e}{2m_e E_R}\right)^{3/2}} \ln\left(\frac{3.45\times10^6\, E_R^2 T_e}{n_e m_R^2}\right) \qquad (2)$$

where n_e and T_e are the number, density, and temperature of the free electrons, respectively. The range of conditions over which the assumption that the free electrons thermalize is valid is discussed in appendix D.

In encounters of beam particles with neutral target atoms, the energy transfers are integrated over a range having the ionization potential of the target material as the lower limit and a head-on collision defining the upper limit of integration. The range of impact parameters for such encounters is on the order of the Bohr radius. When considering energy transfer to free electrons, however, the minimum energy exchange is cut off at an impact parameter corresponding to the Debye length for the case of a charged incident particle. The many events in which appreciable energy is exchanged in this relatively large realm of influence of charged incident particles make the total energy exchange from neutral incident particles to free electrons small in comparison. The energy exchanges from neutral incident particles to free electrons will for ease of calculation be

(slightly pessimistically) neglected herein.

Let f_R be the number of species R particles leaving the reactor per unit time. The energy transfer rate from reactor species R per unit distance x to both bound and free electrons is thus

$$f_R \frac{dE_R}{dx} = -\frac{f_R e^4 \frac{m_R}{m_e}}{16\pi\epsilon^2 E_R} \begin{cases} n_n \dfrac{2\ln\frac{2}{w_R} + \frac{8}{3}}{\left(1 + w_R^2\right)^{3/2}} + \dfrac{n_e (F_{R^+}) \ln\left(\frac{3.45\times10^6 E_R^2 T_e}{n_e m_R^2}\right)}{\sqrt{\frac{\pi}{2}}\left(1 + \frac{m_R k T_e}{2 m_e E_R}\right)^{3/2}} \\ \qquad \text{when } U \le KE_R(1 - w_R) \\ \dfrac{n_n}{\left(1 + w_R^2\right)^{3/2}}\left(\ln\frac{4.825}{w_R} + 1.804 + \frac{0.833}{w_R} - \frac{w_R}{6} - \frac{w_R^3}{96}\right) + \dfrac{n_e (F_{R^+}) \ln\left(\frac{3.45\times10^6 E_R^2 T_e}{n_e m_R^2}\right)}{\sqrt{\frac{\pi}{2}}\left(1 + \frac{m_R k T_e}{2 m_e E_R}\right)^{3/2}} \\ \qquad \text{when } U \ge KE_R(1 - w_R) \end{cases} \tag{3}$$

Conservation Equations of Propellant Species

Continuity of free electrons. - Consider the control volume in Lagrangian coordinates given in figure 2. The free electrons are magnetically confined so that, when diffusion is neglected, the magnetic field lines are envisioned as forming the channel boundaries. A coinciding wall of solid material was assumed adequate to prevent loss of neutral hydrogen atoms.

For a steady process, the number of free electrons created by collisions per unit time inside the control volume equals the net flow of free electrons out of the control volume; that is,

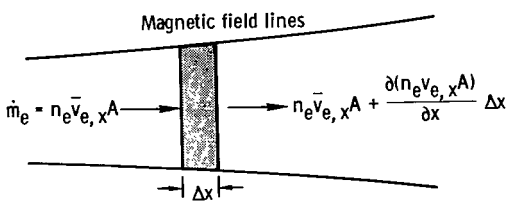

Figure 2. - Control volume for electrons.

$$\frac{\delta}{\delta t}(n_e A\, \Delta x)\bigg|_{coll} = \frac{\partial(n_e \bar{v}_{e,x} A)}{\partial x} \Delta x \tag{4}$$

where $\bar{v}_{e,x} = \bar{v}_{e,x}(x)$ is the mean velocity of the electrons that had their origin in the propellant.

The subscript x denotes that the velocity is in the x direction, that is, along the stream tube axis. The free electrons from the beam make a negligible number of ionizing encounters and thus make no contribution to this equation.

Ionization by beam ions. - The number of ionizing encounters between beam ions and hydrogen neutrals per unit time in a distance Δx is

$$\sum_R f_R n_n Q_R \Delta x$$

where Q_R is the ionization cross section. From equation (C5) it can be written as

$$Q_R = \frac{e^4 \frac{m_R}{m_e}}{16\pi\epsilon^2 E_R U\left(1 + w_R^2\right)^{3/2}} \begin{cases} \frac{5}{3} + \frac{w_R^2}{12} & \text{for } U \le KE_R(1 - w_R) \\ 1.777 - \frac{w_R}{48}\left(w_R^2 - 2w_R + 4\right) & \text{for } U > KE_R(1 - w_R) \end{cases} \tag{5}$$

Ionization by free electrons. - The cumulative effect of encounters between free electrons and hydrogen atoms can contribute to ionization also. The following expression is derived in appendix C for the number of ionizing encounters per unit volume per unit time by free electrons having a Maxwellian velocity distribution:

$$n_n n_e \overline{Qv}_e = \frac{n_n n_e e^4}{4\pi U\epsilon^2 \sqrt{2\pi m_e kT_e}} \left\{ \frac{0.0446}{e^{U/(kT_e)}} \left[1 + \frac{20.95}{e^{U/(kT_e)}} \right] \right\} \tag{6}$$

The continuity equation for free electrons can thus be written

$$\frac{dn_e}{dx} = -\frac{n_e}{\bar{v}_{e,x} A}\left(\bar{v}_{e,x}\frac{dA}{dx} + A\frac{d\bar{v}_{e,x}}{dx}\right) + \frac{n_n n_e e^4}{4\pi U\epsilon^2 \sqrt{2\pi m_e kT_e}\,\bar{v}_{e,x}} \left\{ \frac{0.0446}{e^{U/(kT_e)}} \left[1 + \frac{20.95}{e^{U/(kT_e)}} \right] \right\}$$

$$+ \sum_R \frac{f_R n_n e^4 \frac{m_R}{m_e}}{16\pi A\epsilon^2 \bar{v}_{e,x} U E_R \left(1 + w_R^2\right)^{3/2}} \begin{cases} \frac{5}{3} + \frac{w_R^2}{12} & \text{for } U \le KE_R(1 - w_R) \\ 1.777 - \frac{w_R}{48}\left(w_R^2 - 2w_R + 4\right) & \text{for } U \ge KE_R(1 - w_R) \end{cases} \tag{7}$$

Momentum of free electrons. - The divergence of the magnetic field vector $\vec{B}$ for cylindrical symmetry is

$$\frac{1}{r}\frac{\partial}{\partial r}(rB_r) + \frac{\partial B_x}{\partial x} = 0$$

For slow variations of the magnetic field along the axis of symmetry of any local flux tube,

$$\frac{\partial B_x}{\partial x} \approx \frac{dB}{dx}$$

and the first expression reduces to

$$B_r = -\frac{r}{2}\frac{dB}{dx}$$

In the time interval between collisions, the velocity $v_{e,\perp}$ of free electrons normal to the magnetic field describes arcs of Larmor radii:

$$r = \frac{mv_{e,\perp}}{eB} \tag{8}$$

Substitution of the last two expressions into the Lorentz force equation for the component parallel to the B-field yields

$$\bar{F}_{||} = ev_{e,\perp}B_r = -\frac{m_e v_{e,\perp}^2}{2B}\frac{dB}{dx} \tag{9}$$

The slow B-field change stipulation in this derivation is valid since the electrons make many orbits during only a very small B-field variation in the application herein. Equation (9) is then valid if the collision frequency is small compared with the cyclotron frequency (see appendix D).

Integration of equation (9) over a Maxwellian distribution in the transverse plane yields an average force per electron of

$$\bar{F}_{||} = -\frac{kT_e}{B}\frac{dB}{dx}$$

This force combined with any electrostatic force due to charge separation $-q(d\varphi/dx)$ and the frictional forces due to collisions with hydrogen ions and atoms is balanced by the inertial force on the electrons. Thus,

$$m_e \bar{v}_{e,x} \frac{d\bar{v}_{e,x}}{dx} = -\frac{kT_e}{B}\frac{dB}{dx} + e\frac{d\varphi}{dx} - m_e \nu_{e,i}(\bar{v}_{e,x} - \bar{v}_{i,x}) - m_e \nu_{e,n}(\bar{v}_{e,x} - \bar{v}_{n,x}) \qquad (10)$$

Several underlying assumptions permit the momentum equations to be written in this simple form. Collisions between like particles result in a pressure term that was negligible for the cases of interest when compared with the large electromagnetic terms. Therefore, it is included only in the momentum equation for neutrals. Collisions between unlike particles are accounted for by the "friction terms." These terms are written in the phenomenological form of Schlüter (ref. 14), which involves a difference of mean velocities of the various species and an average momentum transfer collision frequency ν. Also the three propellant species are assumed to have nearly equal mean velocities. This assumption, which will be borne out in later calculations, eliminates a small inertial term accounting for the mass source of a given species due to ionization and charge exchange.

In fact, the coupling between free electrons and hydrogen ions will be assumed to be so close that the velocities (and thus accelerations) of these two species in the x-direction are equal ($\bar{v}_{e,x} = \bar{v}_{i,x} \equiv \bar{v}_x$). Thus, the first friction term in equation (10) is eliminated. This process of accelerating ions by their strong coupling with electrons is sometimes termed "adiabatic acceleration" and is discussed in references 15 to 17. This coupling is not possible unless the electron paths for recirculation, or short circuiting, are eliminated. Thus, for example, any wall used for additional confinement must be nonconducting.

The collision frequency for the remaining friction term was evaluated by the following expression (see pp. 57 and 59 of ref. 13):

$$\nu_{e,n} = \frac{8}{3\sqrt{\pi}} n_n \alpha \int_0^\infty \left(\frac{g}{\alpha}\right)^5 \exp\left(-\frac{g^2}{\alpha^2}\right) \sigma_{e,n}\, d\left(\frac{g}{\alpha}\right)$$

where $g = |\vec{v}_e - \vec{v}_n|$, and as discussed on page 10 of reference 18

$$\alpha = \sqrt{2k\left(\frac{T_n}{m_n} + \frac{T_e}{m_e}\right)}$$

Thus for the study herein

$$\alpha \approx \sqrt{2k \frac{T_e}{m_e}}$$

The momentum transfer cross section $\sigma_{e,n}$ is equal to the total scattering cross section when the "hard sphere" model for neutrals is assumed. A constant value of 0.7×10^{-19} square meter was considered sufficiently representative for $\sigma_{e,n}$ in the energy range of interest (fig. 1.5 of ref. 19 and p. 199 of ref. 20). Integration of the preceding expression then resulted in

$$\nu_{e,n} = 2 \times 10^{-12} n_n \sqrt{T_e} \tag{11}$$

Momentum of protons. - The hydrogen ions (protons) receive very little direct energy from beam particles (see the section entitled Stopping power). They are accelerated by the electrons through the electrostatic potential φ and retarded by their collisions with neutrals. The adiabatic acceleration assumption eliminates the friction term between protons and electrons. The momentum balance in a parallel direction is

$$m_i \bar{v}_i \frac{d\bar{v}_{i,x}}{dx} = -e \frac{d\varphi}{dx} - \frac{m_i}{2} \nu_{i,n} (\bar{v}_{i,x} - \bar{v}_{n,x}) \tag{12}$$

where in this case

$$\nu_{i,n} = \frac{8}{3\sqrt{\pi}} n_n \alpha \int_0^\infty \left(\frac{g}{\alpha}\right)^5 \exp\left(-\frac{g^2}{\alpha^2}\right) \sigma_{i,n} \, d\left(\frac{g}{\alpha}\right)$$

and

$$\alpha = 2 \sqrt{\frac{kT_i}{m_i}}$$

An expression for scattering cross section was obtained by fitting a hyperbola to the data in table I of reference 21 (see fig. 3):

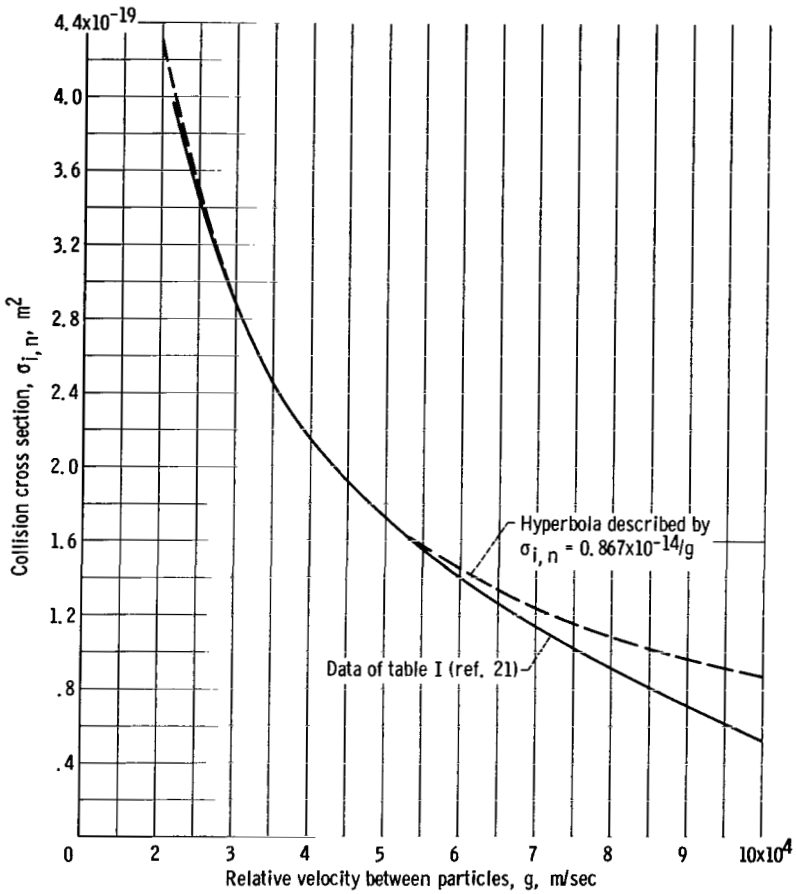

Figure 3. - Elastic scattering of protons in hydrogen.

$$\sigma_{i,n} = \frac{0.867\times10^{-14}}{g}$$

The corresponding expression for collision frequency is

$$\nu_{i,n} = 0.867\times10^{-14}\, n_n \tag{13}$$

Eliminating the electrostatic potential term by substituting equation (10) into equation (12) and using expressions (11) and (13) for collision frequencies result in

$$m_i \bar{v}_x \frac{d\bar{v}_x}{dx} = -\frac{kT_e}{B}\frac{dB}{dx} - m_i n_n (\bar{v}_x - \bar{v}_{n,x})\left(0.433\times10^{-14} + 1.09\times10^{-15}\sqrt{T_e}\right)$$

where $m_i \gg m_e$.

Neglecting diffusion across field lines yields the following relation between flow area and the magnetic field:

$$\frac{B}{B_0} = \frac{A_0}{A} \tag{14}$$

Thus

$$-\frac{1}{B}\frac{dB}{dx} = \frac{1}{A}\frac{dA}{dx}$$

and the preceding momentum equation becomes

$$\frac{d\bar{v}_x}{dx} = \frac{kT_e}{v_x A m_i}\frac{dA}{dx} - 0.433\times10^{-14}\, n_n\left(1 - \frac{\bar{v}_{n,x}}{\bar{v}_x}\right)\left(1 + 0.2512\sqrt{T_e}\right) \tag{15}$$

Momentum of neutral propellant atoms. - The momentum balance for neutrals can be written

$$m_n\bar{v}_{n,x}\frac{d\bar{v}_{n,x}}{dx} = m_e\nu_{n,e}(\bar{v}_x - \bar{v}_{n,x}) + \frac{m_n}{2}\nu_{n,i}(\bar{v}_x - \bar{v}_{n,x}) - \frac{1}{n_n}\frac{dp_n}{dx}$$

Using the previous procedure for evaluating collision frequencies (with $\sigma_{e,n} = \sigma_{n,e}$ and $\sigma_{i,n} = \sigma_{n,i}$) gives

$$\frac{d\bar{v}_{n,x}}{dx} = 0.433\times10^{-14}\, n_e\left(\frac{\bar{v}_x}{\bar{v}_{n,x}} - 1\right)\left(1 + 0.2512\sqrt{T_e}\right) - \frac{kT_n}{m_n\bar{v}_n n_n}\frac{dn_n}{dx} \tag{16}$$

where the equation of state was applied with cold neutrals to the pressure gradient term.

Calculations indicated (Preliminary Results section) that the friction force between the ions and neutrals is very effective in accelerating the neutrals for cases of interest herein, and thus $\bar{v}_x \approx \bar{v}_n$. The acceleration of neutrals would actually be aided further by charge exchange (neglected herein) between these two species of the propellant.

Propellant energy. - The energy added to the propellant by beam particles minus the energy lost by ionization and radiation equals the energy transported away by the propellant. Thus

$$-\sum f_R \frac{dE_R}{dx}\Delta x - U'\frac{\delta}{\delta t}(n_e A\,\Delta x)\Big|_{coll} - p_{brem} A\,\Delta x$$

$$= m_e(c_p)_e\left[n_e\bar{v}_x A\frac{dT_e}{dx} + T_e\frac{d(n_e\bar{v}_x A)}{dx}\right]\Delta x$$

$$+\frac{d}{dx}\left[m_i n_i \bar{v}_x A\left(\frac{\bar{v}_x^2}{2}\right) + m_n n_n \bar{v}_{n,x} A\left(\frac{\bar{v}_{n_x}^2}{2}\right)\right]\Delta x \qquad (17)$$

where

$$m_e(c_p)_e T_e\frac{d(n_e\bar{v}_x A)}{dx}\Delta x = m_e(c_p)_e T_e\frac{\delta}{\delta t}(n_e A\,\Delta x)\Big|_{coll}$$

is the amount of energy to heat the newly formed free electrons to T_e. The loss due to bremsstrahlung is (p. 31, ref. 22)

$$p_{brem} = 5.35\times10^{-37} n_e(n_n + n_e)\sqrt{T_e}$$

where the loss is expressed in Newton-meters per cubic meter and where electron temperature is expressed in kiloelectron volts.

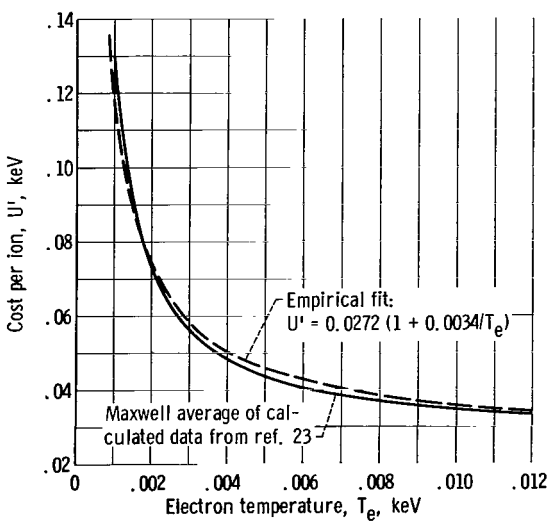

Figure 4. - Cost of ion production by low-temperature electrons.

The cost of forming a hydrogen ion U' by the free electrons is quite high since their average energy is even less than the ionization potential. In this low energy range the probability of exciting a hydrogen atom to a low energy level can be much greater than that of an ionizing encounter. Calculations based on the cross-sectional data of reference 23 and averaged for a Maxwell distribution of incident electron velocity are given in figure 4. The following empirical data fit (shown by the dashed line) will be used in the remaining calculation:

$$U' = 0.0272\left(1 + \frac{0.0034}{T_e}\right) \quad \text{keV}$$

For the relatively high energy ion beam, radiative encounters were neglected, and U' was set equal to 0.0136 kiloelectron volt.

Conservation of Propellant Mass

The flow rate of the total propellant species $\dot{m}$ is

$$\dot{m} = \left[(n_e m_e + n_i m_i)\bar{v}_x + n_n m_n \bar{v}_{n,x}\right]A \approx (n_e m_i \bar{v}_x + n_n m_n \bar{v}_{n,x})A = \text{constant} \qquad (18)$$

since $n_e = n_i$ and $m_e \ll m_i$.

APPLICATION

The preceding equations will now be applied to the species and ranges of conditions pertinent to a conceptual thermonuclear rocket.

Reactor

In the reaction of interest for propulsion applications (refs. 5 and 6) the two isotopes helium 3 and deuterium combine to give off a 3.5 MeV alpha particle and a 14.7 MeV proton. If the energy of these reaction products is expended in heating the incoming fuel, then the number of fuel particles inside the reactor should outnumber the reaction products by a ratio of about 100 to 1. The beam emitted by the weaker mirror would then be essentially composed of only fuel particles.

The flux and initial energies of the beam are dependent on the magnetic mirror system and its particle loss mechanism. The author of reference 24 calculated a large electrostatic potential about a reactor, which was caused by the greater tendency of the electrons relative to that of the ions to scatter into the "loss cones" of the mirrors. The kinetic energy of the electrons is greatly reduced as they emerge, whereas that of the escaping ions could be easily doubled by the electrostatic field. This additional kinetic energy is in a translational mode, the velocity of which is parallel to the axis of symmetry of the reactor.

Of all the ions inside the reactor, however, the lower energy ones are most apt to

TABLE I. - DATA FOR REFERENCE CONFIGURATION

Ion temperature inside reactor, keV	Electron temperature inside reactor, keV	Energy of ions emitted from weaker mirror, $E_{He\text{-}3_0} = E_{D_0}$, keV	Flux of ions emitted from weaker mirror, $f_{He\text{-}3} = f_D$, sec^{-1}	Mass flow of beam, kg/sec	Minimum inside diameter of mirror coils, $D_{m,min}$, m	Initial cross section of ion beam (jet), A_0, m^2
50	38.5	50	0.625×10^{22}	0.522×10^{-4}	1.22	0.0942
100	67.0	100	.312	.261	1.22	.0805

enter the loss cone (p. 351, ref. 22). Thus, the translational energy of the escaping ions is somewhat near their mean thermal energy inside the reactor. In order to size the reactor these two energies will be assumed equal; however, because the precise relation is uncertain, the calculations herein will be identified by values of initial beam energy instead of reactor temperature.

The reactor used is essentially that described in reference 5 and was sized to supply 100 megawatts of power to the escaping ions. Pertinent data are shown in table I for a reference configuration. The reaction zone for this reference configuration was arbitrarily given a length-diameter ratio of 5. For the given total power, this ratio determines the reactor diameter. A shield was inserted between the reactor and the magnet, thus influencing the minimum magnet diameters. A mirror ratio of 4 was used unless stated otherwise.

Magnetic Field Strength

It was assumed that the reactor particles and propellant do not alter the imposed magnetic field. The field near the axis of symmetry of the magnet (fig. 5) was obtained from reference 25. An empirical curve (dashed) was used to express B/B_0 and A/A_0 as a function of x near the axis of symmetry. The resulting expression is

$$\frac{B_0}{B} = \frac{A}{A_0} = \exp\left[-0.231\left(\frac{x}{D_m}\right)^2 + 2.531\,\frac{x}{D_m}\right] \quad \text{for } 0 \leqq \frac{x}{D_m} \leqq 5 \tag{19}$$

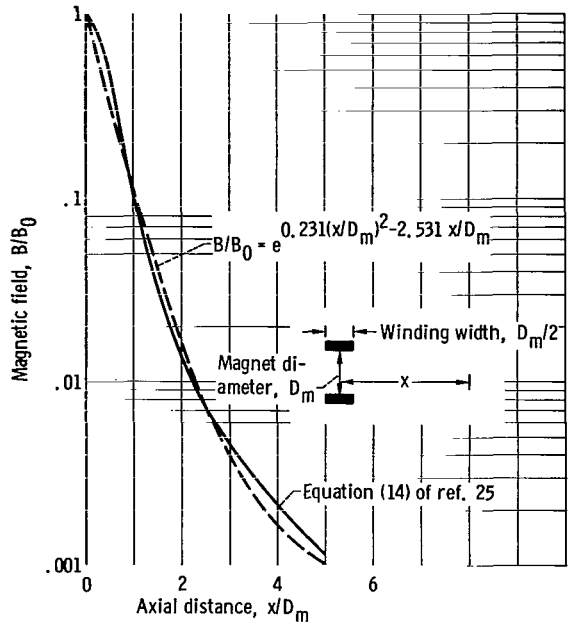

Figure 5. - Magnetic field downstream of reactor mirror on axis of symmetry.

Reduction of Equations

Substituting for the constants in equations (3), (7), (15), (16), (17), and (18), rearranging, and considering two species of ions from the 100-megawatt reactor result in the following set of equations:

$$\frac{dE_{He-3}}{dx} = -\frac{3.585\times10^{-20}}{E_{He-3}} X \qquad \frac{keV}{m} \tag{3a}$$

$$\frac{dE_D}{dx} = -\frac{2.390\times10^{-20}}{E_D} Y \qquad \frac{keV}{m} \tag{3b}$$

$$\frac{dn_e}{dx} = -\frac{n_e}{\bar{v}_x A}\frac{dA}{dx}\left(\bar{v}_x + 0.958\times10^{11}\frac{T_e}{\bar{v}_x}\right) + \frac{0.846\times10^{-7} n_n}{\bar{v}_x} Z + \frac{n_e}{\bar{v}_x} W \tag{7a}$$

$$\frac{d\bar{v}_x}{dx} = \frac{0.958\times10^{11} T_e}{\bar{v}_x}\left(\frac{1}{A}\frac{dA}{dx} - \frac{1}{n_e}\frac{dn_e}{dx} - \frac{W}{A}\right) \tag{15a}$$

$$\frac{d\bar{v}_{n,x}}{dx} = \frac{n_e \bar{v}_x}{n_n \bar{v}_{n,x}} W - \frac{0.958\times10^{11}\, T_n}{n_n \bar{v}_{n,x}} \frac{dn_n}{dx} \tag{16a}$$

$$\frac{dT_e}{dx} = \frac{44.44\, rX}{E_{He-3} \bar{v}_x A n_e} + \frac{29.65\, rY}{E_D \bar{v}_x A n_e} - \frac{1.33\times10^{-21}(n_n + n_e)\sqrt{T_e}}{\bar{v}_x}$$

$$- \frac{0.457\times10^{-9}\, n_n \left[\frac{Z'}{Z} + 185\, T_e + 0.767\times10^{-9}\left(\bar{v}_x^2 - \bar{v}_n^2\right)\right]}{\bar{v}_x n_e} Z - \frac{0.398\, T_e}{A} \frac{dA}{dx}$$

$$+ 0.415\times10^{-11} (\bar{v}_x - \bar{v}_{n,x}) W \tag{17a}$$

$$n_n = \frac{1}{\bar{v}_{n,x}} \left(\frac{0.599\times10^{27}\, \dot{m}}{A} - n_e \bar{v}_x \right) \tag{18a}$$

$$A = A_0 \exp\left[-0.231 \left(\frac{x}{D_m} \right)^2 + 2.531 \frac{x}{D_m} \right] \tag{19}$$

where

$$W = 0.433\times10^{-14}\, n_n \left(1 - \frac{\bar{v}_{n,x}}{\bar{v}_x}\right)\left(1 + 0.2512 \sqrt{T_e}\right) \tag{20}$$

$$X = \frac{n_n}{\left(1 + \frac{74.8}{E_{He-3}}\right)^{3/2}} \begin{cases} \ln\left(\frac{E_{He-3}}{18.7}\right) + 2.667 & \text{when } E_{He-3} \geq 108.8 \\ \frac{1}{2}\ln\left(\frac{E_{He-3}}{3.21}\right) + 1.804 + \frac{\sqrt{E_{He-3}}}{10.37} - \frac{1.442}{\sqrt{E_{He-3}}} - \frac{6.74}{(E_{He-3})^{3/2}} & \text{when } 3.21 \leq E_{He-3} \leq 108.8 \\ 0 & \text{when } E_{He-3} < 3.21 \end{cases}$$

$$+ \frac{n_e F_{He-3^+}}{1.25\left(1 + 2750 \frac{T_e}{E_{He-3}}\right)^{3/2}} \ln \frac{3.502\times10^{27} (E_{He-3})^2\, T_e}{n_e} \tag{21}$$

$$Y = \frac{n_n}{\left(1 + \frac{49.9}{E_D}\right)^{3/2}} \begin{cases} \ln \frac{E_D}{12.47} + 2.667 & \text{when } E_D \geq 72.5 \\ \frac{1}{2} \ln \frac{E_D}{2.14} + 1.804 + \frac{\sqrt{E_D}}{8.48} - \frac{1.167}{\sqrt{E_D}} - \frac{3.668}{(E_D)^{3/2}} & \text{when } 2.14 \leq E_D \leq 72.5 \\ 0 & \text{when } E_D < 2.14 \end{cases}$$

$$+ \frac{n_e F_{D^+}}{1.25\left(1 + 1833 \frac{T_e}{E_D}\right)^{3/2}} \ln \frac{7.92 \times 10^{27} (E_D)^2 T_e}{n_e} \qquad (22)$$

$$Z = \frac{0.977 \times 10^{11} r}{E_{He-3} A \left(1 + \frac{74.8}{E_{He-3}}\right)^{3/2}} \begin{cases} \frac{5}{3} + \frac{6.23}{E_{He-3}} & \text{when } E_{He-3} \geq 108.8 \\ 1.777 - \frac{0.1801}{\sqrt{E_{He-3}}} \left(\frac{74.8}{E_{He-3}} - \frac{17.30}{\sqrt{E_{He-3}}} + 4\right) & \text{when } 3.21 \leq E_{He-3} \leq 108.8 \\ 0 & \text{when } E_{He-3} < 3.21 \end{cases}$$

$$+ \frac{0.652 \times 10^{11} r}{E_D A \left(1 + \frac{49.9}{E_D}\right)^{3/2}} \begin{cases} \frac{5}{3} + \frac{4.157}{\sqrt{E_D}} & \text{when } E_D \geq 72.5 \\ 1.777 - \frac{0.147}{\sqrt{E_D}} \left(\frac{49.9}{E_D} - \frac{14.12}{\sqrt{E_D}} + 4\right) & \text{when } 2.14 \leq E_D \leq 72.5 \\ 0 & \text{when } E_D < 2.14 \end{cases}$$

$$+ \frac{0.538 \times 10^{-8} n_e}{\sqrt{T_e}} e^{-\frac{0.0136}{T_e}} \left(1 + 20.95\, e^{-\frac{0.0136}{T_e}}\right) \qquad (23)$$

$$Z' = Z + \frac{0.538\times10^{-8}\, n_e}{\sqrt{T_e}}\, e^{-\frac{0.0136}{T_e}} \left(1 + 20.95\, e^{-\frac{0.0136}{T_e}}\right)\left(1 + \frac{0.0068}{T_e}\right) \tag{24}$$

$$F_{He\text{-}3^+} = 1.036 - \sqrt{1 - F_{H^+}^2} + \left(2.667\sqrt{1 - F_{H^+}^2} + 2.221\, F_{H^+} - 2.319\right)\frac{E_{He\text{-}3}}{100} \tag{25}$$

$$F_{D^+} = F_{H^+} + 0.375\left(1 - F_{H^+}\right)\frac{E_D}{100} \tag{26}$$

$$F_{H^+} \equiv \frac{n_e}{n_e + n_n}$$

The energies of the reactor particles are given in kiloelectron volts instead of joules in these final equations.

RESULTS AND DISCUSSION

Preliminary Results

Simultaneous solution of the preceding conservation equations for the propellant and the beam was made on a high-speed digital computer.

The early calculations indicated that $\bar{v}_{n,x}/\bar{v}_x$ was so close to unity that the computing process was made difficult because of the loss of significant figures when subtracting $\bar{v}_{n,x}/\bar{v}_x$ from 1 in equation (20). Physically this was due to the very effective acceleration of neutrals by the hydrogen ions for the cases of interest. In all later calculations $\bar{v}_{n,x}/\bar{v}_x$ was set equal to 1. Equations (15a) and (16a) were, therefore, replaced by

$$\frac{d\bar{v}_x}{dx} = \frac{n_e kT_e}{\dot{m}}\frac{dA}{dx}$$

Computations were also facilitated by assuming a slightly nonzero initial fractional ionization of the propellant F_{H^+}. Results were insensitive to a range of initial F_{H^+} from 10^{-7} to 10^{-5}. A value of 10^{-5} was thus selected.

To establish an initial condition, it was assumed that the flow of hydrogen propellant was choked at the injection station. The results did not change appreciably as the hydro-

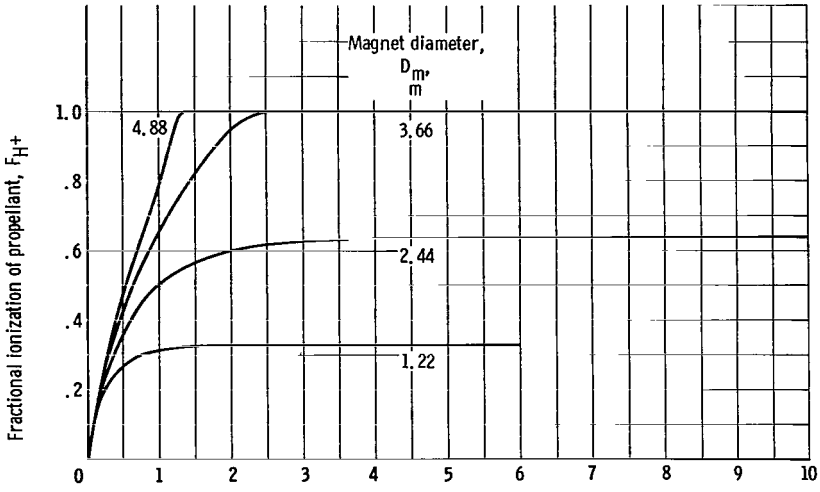

(a) Fractional ionization of propellant.

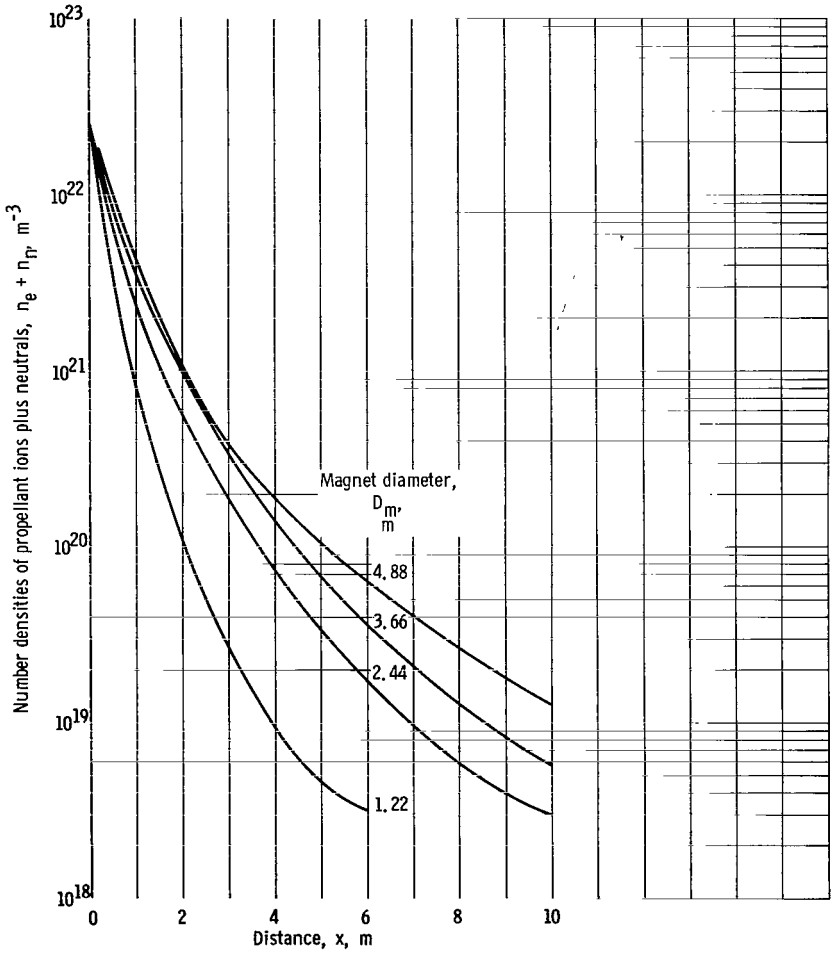

(b) Propellant density.

Figure 6. - Variation of propellant and beam parameters with distance. Initial beam energy, 50 keV; mass flow rate, 0.010 kilogram per second; cross-sectional area of jet, 0.0942 square meter.

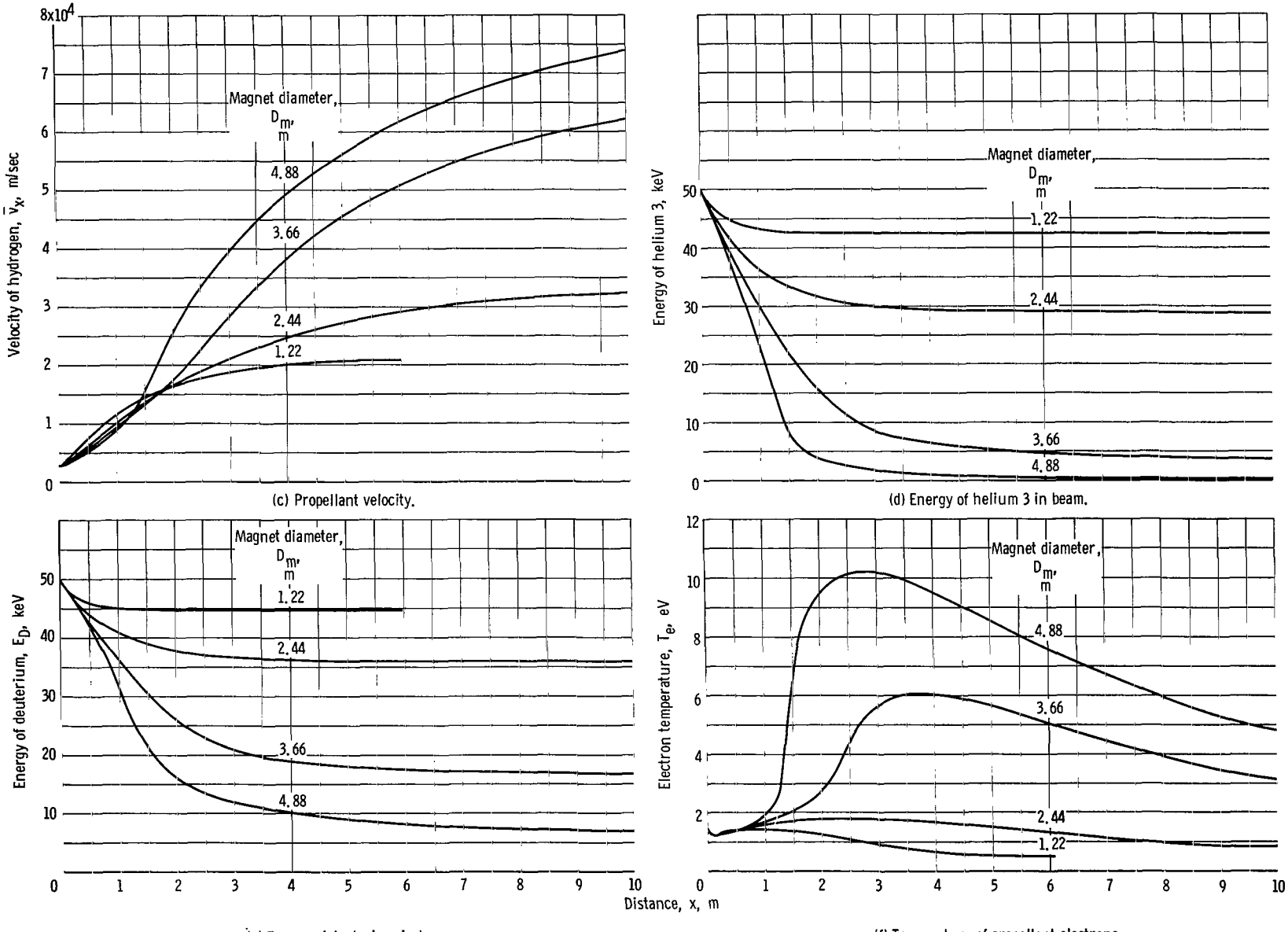

Figure 6. - Concluded.

gen temperature leaving the shield was increased from 1000^{o} to 2000^{o} C. A temperature of 1000^{o} C was used in the remaining calculations.

Preliminary calculations indicated that the temperature of the propellant electrons was so low that loss of energy by bremsstrahlung was negligible.

Dependence of Typical Results on Distance x

A convenient way of varying magnetic field gradient while retaining equation (19) is by varying D_m. The variation of propellant and beam parameters with distance x is shown in figure 6 for four different magnet diameters. Ionization of the propellant is most rapid at low values of x where the propellant density is high and where large amounts of energy can be transferred from the beam (fig. 6(a)). Density decreases very rapidly with distance x (fig. 6(b)) because of the increasing velocity (fig. 6(c)) and the increasing cross-sectional area of the flux tube. Beyond a distance of about one magnet diameter downstream of the injection station, the velocity increased, and the target density decreased to such an extent that little additional energy transfer took place (figs. 6(d) and (e)). The fractional ionization then stays essentially constant; however, acceleration continues for about two more magnet diameters because of the continuing high gradient of the magnetic field (fig. 5) interacting with the remaining energy $n_e kT_e$ in the propellant electrons. The decrease of electron temperature in this region (as the random energy of the electron gas is converted to a rearward directed mean motion) can be seen in figure 6(f).

The large effect of magnet size demonstrated in figure 6 is due to the fact that a larger magnet permits a more gradual decrease in field strength and thus a slower decrease of target density with distance x. Therefore, greater amounts of energy are transferred from the beam. The smaller field gradient of a larger magnet gives less propellant acceleration at low values of x; however, acceleration continues over a greater distance. This extended acceleration and the larger amount of energy exchange result in a net gain in propellant velocity at large values of x.

Thrust is defined herein as the component of momentum in the direction of the axis of symmetry and can be written as

$$\mathcal{F} = (\dot{m}_{He-3} v_{He-3} + \dot{m}_D v_D + \dot{m}\bar{v}_x)\cos_{av}\theta$$

The residual momentum of the reactor particles

$$\dot{m}_{He-3} v_{He-3} + \dot{m}_D v_D$$

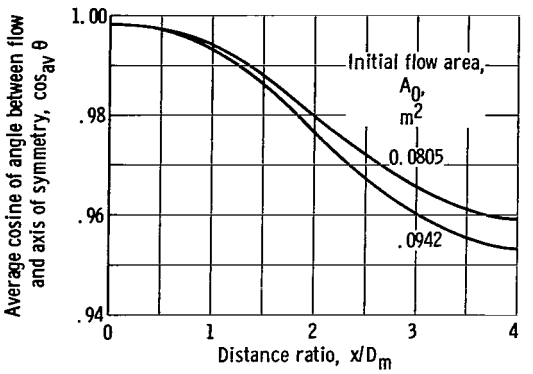

Figure 7. - Variation of flow divergence with distance.

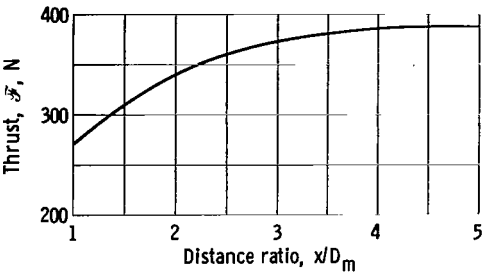

Figure 8. - Dependence of thrust on the axial station at which it is calculated. Magnet diameter, 2.44 meters; propellant flow rate, 0.01 kilogram per second; initial beam energy, 50 keV; initial beam area, 0.0942 square meter.

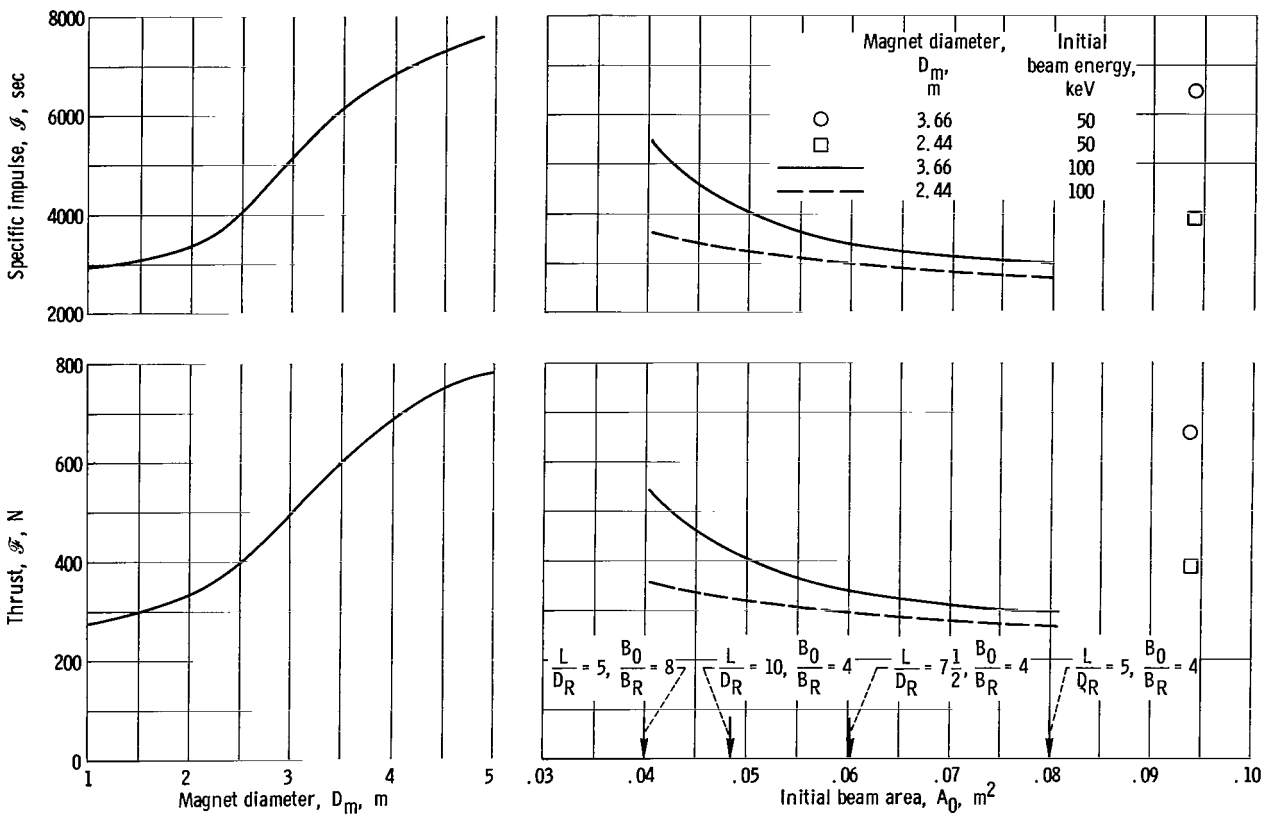

(a) Effect of magnet size. Initial beam area, 0.0942 square meter; initial beam energy, 50 keV.

(b) Effect of initial beam area.

Figure 9. - Jet performance at hydrogen flow rate of 0.01 kilogram per second.

is of significance only at the lowest flow rates of hydrogen. The average cosine of the angle between the propellant flow and the axis of symmetry was weighted on a basis of area normal to the flow. The expression used herein, exact for ideal conical nozzle flow (ref. 26), is

$$\cos_{av}\theta = \frac{1 + \cos\theta_b}{2}$$

where θ_b is the angle between the outer or bounding flux line and the axis of symmetry. Plots of $\cos_{av}\theta$ against distance x are shown in figure 7. Beyond a value for x/D of 3, the decrease of $\cos_{av}\theta$ quite closely balances the small increase of $\bar{v}_x$. Thus beyond this distance it makes little difference at what x station thrust is calculated (fig. 8). Results should therefore be quite insensitive to the location at which the high-velocity jet eventually diffuses across the weak field lines and detaches from the magnetic field.

Jet Performance

Specific impulse is defined in terms of thrust and total mass flow in the jet as

$$\mathit{I} = \frac{\mathit{F}}{(\dot{m}_{He\text{-}3} + \dot{m}_D + m)\mathit{g}}$$

The product of I times the acceleration of gravity g is the mean effective velocity of the jet.

The dependence of F and I on magnet size and initial beam area A_0 is shown in figure 9. Figure 9(a) is based on the data of figure 6 at a distance x of 10 meters. The large influence of magnet diameter D_m is again demonstrated. The only influence of magnet strength in the calculations is through its effect on the size of the cross-sectional area of the beam and magnetic flux tube. Increasing the mirror ratio for the same reactor diameter decreases A_0 according to equation (14). Also for the same reactor volume, A_0 can be decreased by using a longer and more slender reactor (greater length-diameter ratio L/D_R). For example, A_0 can be cut in half by either doubling the mirror ratio or by increasing the length-diameter ratio of the reaction zone L/D_R by a factor of 2.8. Various pertinent combinations of B_0/B_R and L/D_R are indicated on the abscissa of figure 9(b). Reducing the cross-sectional area of the interaction region for the same hydrogen flow, beam flux, and energy results in an increase in energy transfer. In general, figure 9(b) shows that decreasing A_0 increases both F and I

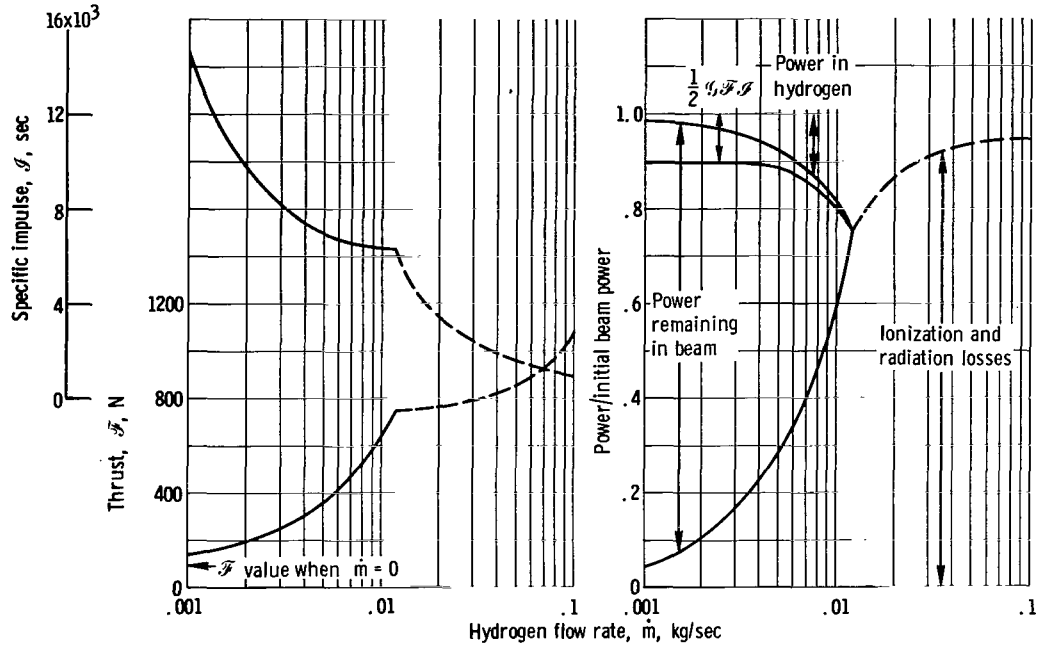

Figure 10. - Effect of propellant flow rate on jet performance. Initial beam energy, 50 keV; magnet diameter, 3.66 meters; initial beam area, 0.0942 square meter; distance, x, 10 meters.

over the range of variables studied.

The effect of initial beam energy can be seen by comparing figures 9(a) and (b). The four data points in figure 9(b) represent performance at an initial beam energy of 50 keV. The beam area for the 100-keV case would have to be reduced to about one-third of its original value to bring the thrust and specific impulse up to that of the 50-keV case. These results typify the inverse dependence of energy transfer rate on beam energy level as determined by equation (3).

The influence of propellant flow rate on jet performance is shown in figure 10. Increase of $\dot{m}$ increases $\mathcal{F}$ but decreases $\mathcal{I}$. As $\dot{m}$ is increased, the target density is increased to a condition where the beam is able to transfer essentially all its energy to the target. Beyond this point the acceleration of the hydrogen continues as the magnetic field gradient converts the residual $n_e kT_e$ to directed translational energy. The location where the beam runs out of energy is apparent by the abrupt change in slope of the curves in figure 10. To save computing time, the calculations were completed with the remaining neglibible energy set equal to zero, when the energies of both species of reactor particles fell below 0.05 keV.

The power that is useful for propulsion is often defined as $\frac{1}{2}\mathcal{F}\mathcal{I}$. The ratio of this jet power to initial power in the beam is shown in figure 10. Also shown is the kinetic energy in the hydrogen alone, the energy remaining in the beam that could not be transferred to the hydrogen propellant, and the cost of ionizing the propellant, which includes radiative encounters. For this case, the maximum overall efficiency of the

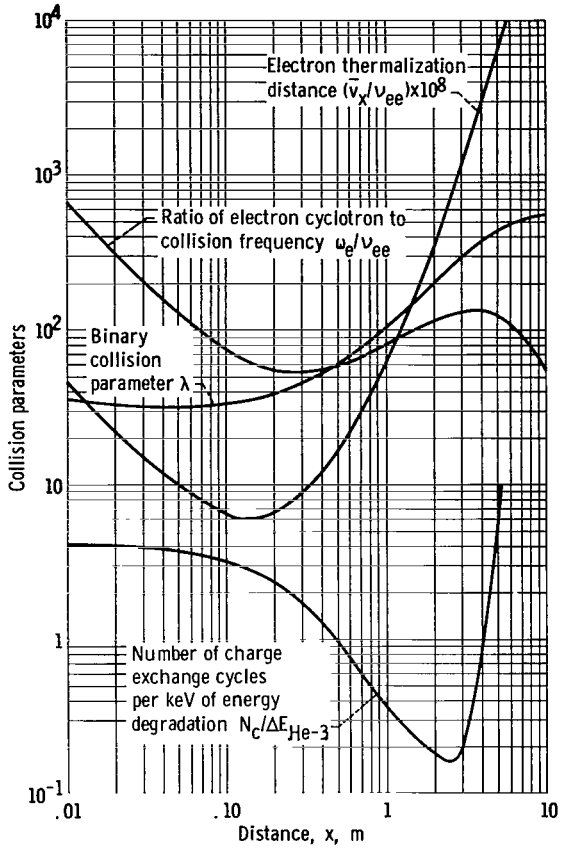

Figure 11. - Collision parameters. Initial energy of beam, 50 keV; initial magnetic field strength, 20.8 Webers per square meter; hydrogen flow rate, 0.010 kilogram per second; magnet diameter, 2.44 meters.

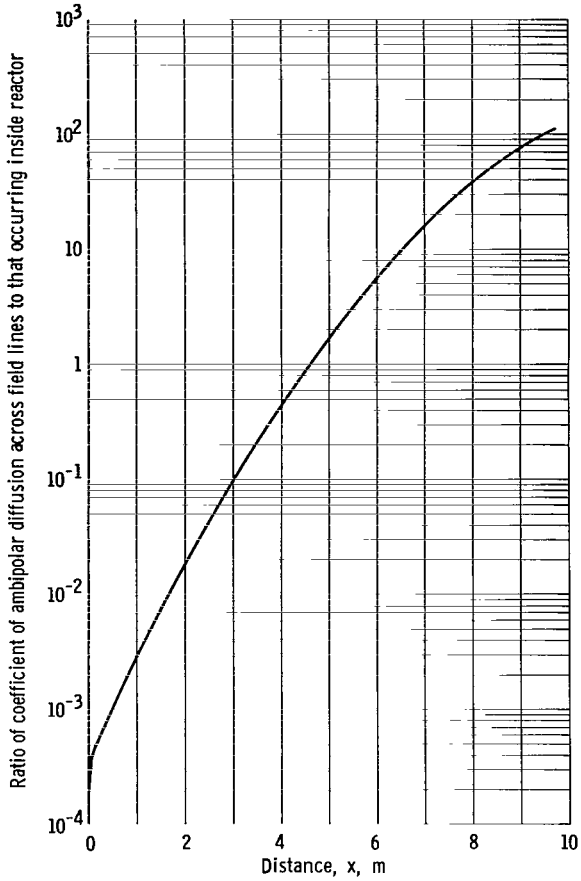

Figure 12. - Variation of diffusion parameter with distance. Initial energy of beam, 50 keV; magnet diameter, 2.44 meters; hydrogen flow rate, 0.010 kilogram per second.

energy transfer and acceleration process was calculated to be 25 percent. This maximum occurred near an $\dot{m}$ of 0.01 kilogram per second. At this point of maximum efficiency, the jet thrust was more than seven times that of the beam alone. At low hydrogen flow rates only a small amount of power from the beam could be transferred to the target. At high flow rates loss is mainly due to power consumed in ionizing the hydrogen.

Appraisal of Assumptions

The computed data, such as that presented in figure 6, permit appraisal of several of the assumptions regarding collisions discussed in the ANALYSIS section. Details are given in appendix D and results are plotted in figures 11 and 12 for a typical set of conditions. Parameters are presented that are useful for judging the validity of the assumptions of binary collisions, thermalization of free electrons, beam equilibration, and the

expression for the magnetic force on free electrons. As discussed in appendix D, results are, in general, quite favorable to the methods used in the analysis. Loss of charged particles by ambipolar diffusion across the flux tube (fig. 12) appears to be a much lesser problem than that occurring inside the reactor. The large values of diffusion coefficient for large values of x permit the high-velocity jet to diffuse eventually across the magnetic field lines, which it must do to produce thrust.

CONCLUSIONS

The acceleration of a hydrogen propellant along a magnetic tube of flux by use of high-energy beams of light-weight ions was studied. Subject to the assumptions and simplifications in the analysis, and for the range of variables studied, the following results were obtained:

1. Energy transfer was most effective when the beam was concentrated on a dense, closely confined target. Thus, increase of propellant mass flow and decrease of initial beam cross-sectional area improved results. Ionization of the hydrogen was usually quite rapid near the station where the beam first impinged on the target. For the cases studied, this was also the location of minimum cross section for the confines of the propellant flow.

2. For the case of a magnetic field generated by a short solenoid, the divergence, or spreading, of the flux tube depends to a large extent on the solenoid diameter. Increasing the diameter of such a magnet permitted suitable energy exchanges over longer distances of beam travel. Beyond a distance of about one magnet diameter downstream of the minimum cross-sectional station, the velocity increased and density decreased such that little further energy transfer could take place. Some acceleration of the hydrogen continued for about another two magnet diameters because of the continuing high magnetic field gradient interacting with the remaining energy of the propellant electrons.

3. An optimum hydrogen flow rate was found where the momentum (thrust) of the propellant could be increased to seven times that initially in the beam and with an overall efficiency of energy transfer of 25 percent. At low hydrogen flow rates, only a small amount of energy could be transferred from the beam to the target. At high flow rates, loss was mainly due to power consumed in ionizing the hydrogen.

4. Bremsstrahlung was negligible since electron temperature was always below 11 eV. Sizable radiation losses were calculated, however, because of the high number of excitation encounters between these electrons and the hydrogen atom.

Lewis Research Center,
National Aeronautics and Space Administration,
Cleveland, Ohio, June 24, 1966.
120-27-06-04-22.

APPENDIX A

SYMBOLS

[The mks system of units is used unless otherwise specified.]

A	cross-sectional area of jet
B	magnetic field intensity
c_p	specific heat at constant pressure for an ideal electron gas, 0.441×10^{15} J/(kg)(keV)
D	diameter
D_m	magnet diameter (see fig. 5)
$\mathscr{D}$	coefficient of ambipolar diffusion
E	energy per particle
e	unit of charge, 1.60206×10^{-19} C
F	equilibrium fraction
$\mathscr{F}$	thrust, N
f	flux of particles
$\mathscr{g}$	acceleration of gravity
g	magnitude of relative velocity between two particles
$\mathscr{I}$	specific impulse
K	$4m_e m_R/(m_e + m_R)^2$
k	Boltzmann constant, 1.6×10^{-16} joules/keV
L	reactor length
m	mass per particle
$\dot{m}$	mass flow rate (without subscript it is for the hydrogen propellant)
n	number density
p	pressure
Q	ionization cross section
r	$f_r/(f_r)$ at a reactor temperature of 100 keV
T	temperature, keV, unless otherwise stated
t	time
U	ionization potential for atomic hydrogen, 0.0136 keV
U'	cost of producing a hydrogen ion
v	velocity
W	defined by expression (20)
w_R	ratio of target particle (electron) velocity to incident R particle velocity
X	defined by expression (21)
x	distance from station of minimum jet area (and hydrogen injection station) along a magnetic field line
Y	defined by expression (22)
Z	defined by expression (23)
z	charge
α	mean thermal speed
ϵ	capacity of a vacuum, 8.854×10^{-12} F/m
θ	angle between a streamline and the axis of symmetry

λ ratio of mean to minimum distance between particles

$\nu_{\ell,m}$ collision frequency between species ℓ and m

$\sigma_{\ell,m}$ momentum transfer cross section between species ℓ and m

φ electrostatic potential

ω cyclotron frequency

Subscripts:

av average

brem bremsstrahlung

coll collision

cx charge exchange

D deuterium

e electrons

H hydrogen

He helium

He-3 helium 3

I ionization

i ion

max maximum

min minimum

n neutral target particle

R beam or reactor

t target

x component in x direction

0 station where beam first impinges on the target, x = 0

$\perp$ perpendicular to magnetic field lines

$\parallel$ parallel to magnetic field lines

Superscripts:

o neutral

. total time differentiation

$\bar{}$ mean mass motion

$\rightarrow$ vector quantity

+ single charge

APPENDIX B

EQUILIBRIUM COMPOSITION OF BEAMS

The following derivations follow quite closely the theory in section B of reference 9 except that in the present case a partially ionized target was used. Also the cross-sectional area and velocity of the beam herein are not constant. The continuity equation for the singly charged helium beam species, for example, can be written as

$$\frac{1}{v_{He} A} \frac{d}{dx}\left(n_{He^+} v_{He} A\right) = \sigma_{cx}^{o,+} n_{He^o} n_{H^+} + \sigma_I^{'o,+} n_{He^o} n_{H^o} + \sigma_I^{o,+} n_{He^o} n_{H^+} - \sigma_{cx}^{+,o} n_{He^+} n_{H^o}$$

where, for example, $\sigma_{cx}^{o,+}$ is a charge exchange cross section in which the charge of the incident particle is changed from 0 to 1. The interacting species to which such a cross section corresponds are labeled on the immediately following number densities in this equation. The subscript I denotes an ionizing encounter. It was assumed that the incident particles undergo frequent enough charge exchange and ionization events that $v_{He^o} = v_{He^+}$. Also the propellant velocity was usually so much lower than the beam velocity that the former was neglected.

Sufficient data to adequately determine $\sigma_I^{'o+}$ were not available. It is therefore assumed herein (as in the ANALYSIS section) that a light neutral is as effective in undergoing an ionizing encounter with a neutral atom as it is after taking on a single charge. Thus, in the above equation

$$\sigma_I^{'o,+} = \sigma_I^{o,+}$$

If the beam equilibrates at a certain composition so that the number of neutralizing events is balanced by the number of ionization encounters, then

$$\frac{d}{dx}\left(n_{He^+} v_{He} A\right) = 0$$

Dividing the right side of the former equation by $\left(n_{He^+} + n_{He^o}\right)\left(n_{H^+} + n_{H^o}\right)$ and defining

$$F_{He^+} = \frac{n_{He^+}}{n_{He^+} + n_{He^o}} \equiv \text{fractional ionization of the helium beam}$$

and

$$F_{H^+} = \frac{n_{H^+}}{n_{H^+} + n_{H^O}} \equiv \text{fractional ionization of the hydrogen propellant}$$

$$= \frac{n_e}{n_e + n_n}$$

result in

$$\sigma_{cx}^{O,+} F_{He^O} F_{H^+} + \sigma_I^{O,+} F_{He^O} - \sigma_{cx}^{+,O} F_{He^+} F_{H^O} = 0$$

where

$$F_{He^O} + F_{He^+} = 1$$

$$F_{H^O} + F_{H^+} = 1$$

Solving for F_{He^+} yields

$$F_{He^+} = \frac{\sigma_{cx}^{O,+} F_{H^+} + \sigma_I^{O,+}}{\sigma_{cx}^{O,+} F_{H^+} + \sigma_I^{O,+} + \sigma_{cx}^{+,O}\left(1 - F_{H^+}\right)} \tag{B1}$$

This expression approaches the result of reference 9 as F_{H^+} approaches zero. The data of references 9 and 27 were then used to determine the preceding cross sections in terms of the energy of the helium beam. The results are shown on figure 13(a). The basic parameter is the relative velocity between incident and target particles and not the energy, which is more convenient to use. The corresponding energy of helium 3 particles is also shown in figure 13(a), wherein it is assumed that the absence of one neutron in the helium nucleus does not alter the basic interaction based on relative velocities. The calculated data are on a per atom basis while the experimental data are for a target of molecular hydrogen.

Similar results can be obtained for protons in hydrogen by using the data of refer-

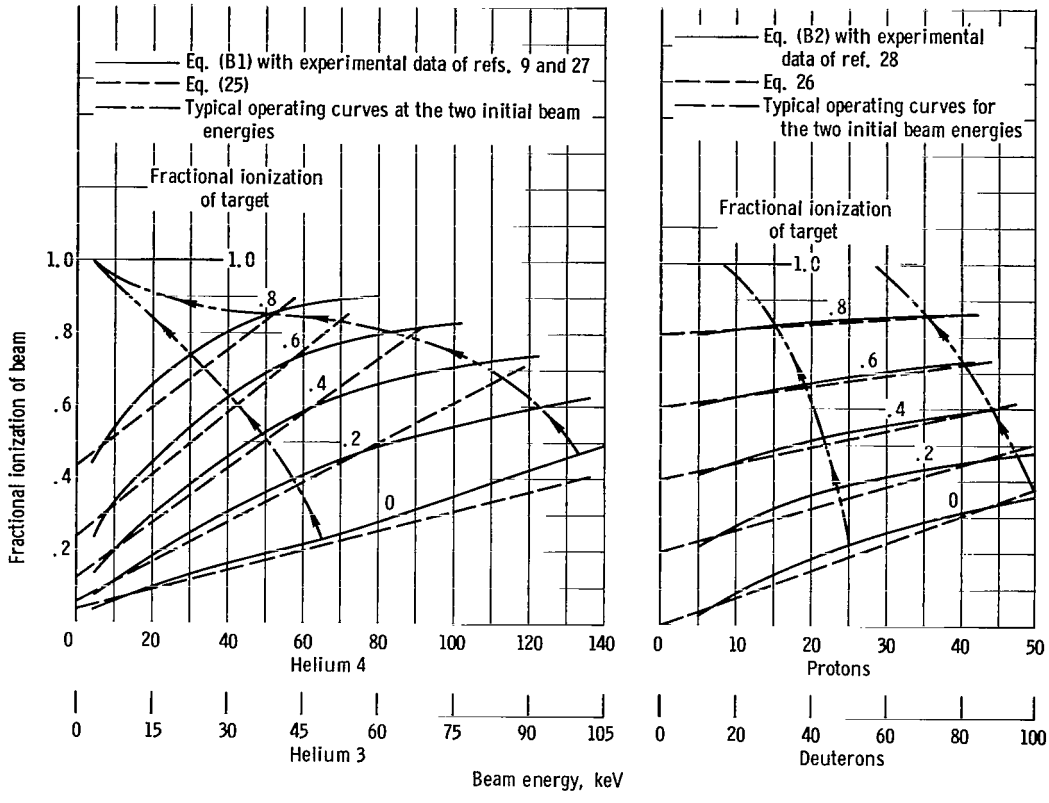

(a) Helium beams in hydrogen target. (b) Hydrogen beams in hydrogen target.

Figure 13. - Equilibrium fractional ionization of beam.

ence 28. These results were used for a deuterium beam impinging on hydrogen. In these cases, however, the charge exchange cross sections should be symmetrical; that is, $\sigma_{cx}^{o,+} = \sigma_{cx}^{+,o}$, which resulted in

$$F_{D^+} = \frac{\sigma_{cx}^{o,+} F_{H^+} + \sigma_I^{o,+}}{\sigma_{cx}^{+,o} + \sigma_I^{o,+}} \tag{B2}$$

(Results are shown in figure 13(b).)

The following empirical fits were made to the final results for convenience in later computations:

$$F_{He\text{-}3^+} = 1.036 - \sqrt{1 - F_{H^+}^2} + \left(2.667\sqrt{1 - F_{H^+}^2} + 2.221\, F_{H^+} - 2.319\right)\frac{E_{He\text{-}3}}{100} \tag{25}$$

$$F_{D^+} = F_{H^+} + 0.375\left(1 - F_{H^+}\right)\frac{E_D}{100} \tag{26}$$

These expressions are shown by the dashed curves in figure 13. The empirical fits deviate as much as 15 percent from the calculated results at some of the higher beam energies. This, however, is close to the experimental scatter of the basic experimental cross sections.

APPENDIX C

ENERGY TRANSFER AND IONIZATION CROSS SECTIONS

The theory of classical particles is used to determine the energy transfer from beam ions to the electrons bound in the hydrogen atoms and also to the free electrons liberated from the hydrogen atoms. This theory is also used to determine cross sections for ionization of hydrogen by the beam ions and by the free electrons. Since all incident particles of this appendix have a positive charge, the + superscript used in the ANALYSIS section has been deleted.

Energy Transfer to Bound Electrons

In this case the mass of the target particle m_e is much less than that of the incident particle m_R. The cross section $\sigma(\Delta E)$ for the transfer of the amount of energy ΔE is given by equation (24) of reference 2. After correcting several algebraic errors (see appendix of ref. 29) it can be written in mks units as

$$\sigma(|\Delta E|) \approx -\frac{z_R^2 e^4 \frac{m_R}{m_e}}{16\pi\epsilon^2 E_R (\Delta E)^2 \left(1 + \frac{v_e^2}{v_R^2}\right)^{3/2}} \begin{cases} 1 + \frac{4}{3}\frac{E_e}{|\Delta E|} & \text{when } |\Delta E| \le KE_R\left(1 - \frac{v_e}{v_R}\right) \\ \frac{1}{2}\left[\sqrt{1 + \frac{|\Delta E|}{E_e}}\left(\frac{1}{3} + \frac{4}{3}\frac{E_e}{|\Delta E|}\right) + \left(1 + \frac{4}{3}\frac{E_e}{|\Delta E|}\right) + \frac{1}{6}\frac{v_e}{v_R}\frac{(\Delta E)^2}{KE_e E_R}\right] & \text{when } |\Delta E| \ge KE_R\left(1 - \frac{v_e}{v_R}\right) \end{cases} \quad \text{(C1)}$$

Absolute value signs have been used to avoid confusion since reference 2 uses $-\Delta E$ as the loss of energy from particle R to particle e, which is opposite to the sign convention elsewhere in this report.

Equation (C1) is then substituted into the following relation for stopping cross section:

$$\frac{1}{n_n}\frac{dE_R}{dx} = \int_U^{|\Delta E|_{max}} \sigma\left(|\Delta E|\right)|\Delta E| \, d\left(|\Delta E|\right)$$

where for a head-on collision (eq. (15) of ref. 2)

$$|\Delta E|_{max} = KE_R\left(1 + \frac{v_e}{v_R}\right)\left(1 - \frac{m_e v_e}{m_R v_R}\right) \approx KE_R\left(1 + \frac{v_e}{v_R}\right) \qquad \text{(C2)}$$

After a tedious integration, the stopping power expression becomes

$$\frac{1}{n_n}\frac{dE_R}{dx} = -\frac{z_R^2 e^4 \frac{m_R}{m_e}}{16\pi\epsilon^2 E_R\left(1 + \frac{v_e^2}{v_R^2}\right)^{3/2}} \left\{ \begin{array}{l} \left(\ln|\Delta E| - \frac{4}{3}\frac{E_e}{|\Delta E|}\right)_U^{KE_R\left(1 - \frac{v_e}{v_R}\right)} + \left[\sqrt{1 + \frac{\Delta E}{E_e}}\left(-\frac{2}{3}\frac{E_e}{|\Delta E|} + \frac{1}{3}\right)\right. \\ \qquad + \frac{1}{2}\ln\left(|\Delta E|\frac{\sqrt{1 + \frac{|\Delta E|}{E_e}} - 1}{\sqrt{1 + \frac{|\Delta E|}{E_e}} + 1}\right) - \frac{2}{3}\frac{E_e}{|\Delta E|} \\ \qquad \left. + \frac{1}{24}\frac{v_e}{v_R}\frac{|\Delta E|^2}{KE_e E_R}\right]_{KE_e\left(1 - \frac{v_e}{v_R}\right)}^{KE_R\left(1 + \frac{v_e}{v_R}\right)} \quad \text{when } U \le KE_R\left(1 - \frac{v_e}{v_R}\right) \\ \left[\sqrt{1 + \frac{|\Delta E|}{E_e}}\left(-\frac{2}{3}\frac{E_e}{|\Delta E|} + \frac{1}{3}\right) + \frac{1}{2}\ln\left(|\Delta E|\frac{\sqrt{1 + \frac{|\Delta E|}{E_e}} - 1}{\sqrt{1 + \frac{|\Delta E|}{E_e}} + 1}\right)\right. \\ \qquad \left. - \frac{2}{3}\frac{E_e}{|\Delta E|} + \frac{1}{24}\frac{v_e}{v_R}\frac{|\Delta E|^2}{KE_e E_R}\right]_U^{KE_R\left(1 + \frac{v_e}{v_R}\right)} \quad \text{when } U \ge KE_R\left(1 - \frac{v_e}{v_R}\right) \end{array} \right.$$

Substituting the limits of integration and reducing in terms of v_e/v_R with $E_e = U$ for the hydrogen atom result in the following equation for singly charged incident particles:

$$\frac{1}{n_n}\frac{dE_R}{dx} = -\frac{e^4\frac{m_R}{m_e}}{16\pi\epsilon^2 E_R\left(1+\frac{v_e^2}{v_R^2}\right)^{3/2}}\begin{cases} 2\left(\ln\frac{2}{\frac{v_e}{v_R}}\right)+\frac{8}{3} & \text{when } U \le KE_R\left(1-\frac{v_e}{v_R}\right) \\ \frac{1}{2}\ln\left[\frac{4}{\left(\frac{v_e}{v_R}\right)^2}\frac{\sqrt{2}+1}{\sqrt{2}-1}\right]+\frac{1}{3}\left[4+\sqrt{2}+\frac{5}{2\frac{v_e}{v_R}}\right. & \\ \qquad \left. -\frac{1}{2}\left(\frac{v_e}{v_R}\right)-\frac{1}{32}\left(\frac{v_e}{v_R}\right)^3\right] & \text{when } U \ge KE_R\left(1-\frac{v_e}{v_R}\right) \end{cases} \tag{C3}$$

Only a small amount of data (figs. 14(a) and (b)) was found for the stopping power of species close to those of interest in the desired energy range. Results of equation (C3) should be compared first with the partial stopping power data of figure 14(a), which is for charged incident particles. Agreement appears satisfactory for present purposes.

In the beam composition discussion of the ANALYSIS section, the assumption was made that the neutral incident particles are as effective as singly charged incident particles in transferring energy to the neutral target particles. This assumption appears reasonable but slightly optimistic in figure 14(b). No contribution to stopping power due to charge exchange was included in the analysis, which is a somewhat pessimistic assumption. Comparison of the total stopping power (diamond symbols) with the results of equation (C3) indicates that the use of equation (C3) for energy loss rate should be reasonable.

Energy Transfer to Free Electrons

From pages 114 and 118 of reference 13

$$\frac{1}{n_e}\frac{dE_R}{dx} = -\frac{1}{2\sqrt{\pi}}\frac{z_R^2 e^4}{\pi\epsilon^2}\frac{k(T_R - T_e)}{v_R m_e m_R\left(\frac{2kT_R}{m_R}+\frac{2kT_e}{m_e}\right)^{3/2}}\ln\left(\frac{|\Delta E|_{max}}{|\Delta E|_{min}}\right)$$

The maximum energy exchange expression (eq. (C2)) can be reduced further here since

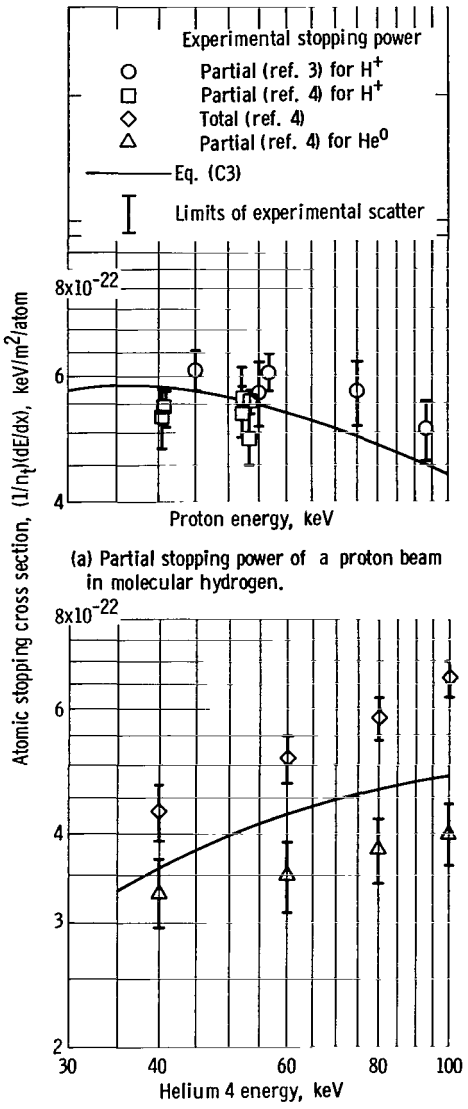

(a) Partial stopping power of a proton beam in molecular hydrogen.

(b) Helium beams in molecular hydrogen.

Figure 14. - Comparison of experimental and theoretical stopping power cross sections.

it occurs in the argument of a slowly varying log function:

$$|\Delta E|_{max} \approx \frac{4m_e}{m_R} E_R$$

The minimum energy exchange $|\Delta E|_{min}$ was determined by setting the impact parameter equal to the Debye length (p. 82 of ref. 13) so that

$$\frac{|\Delta E|_{max}}{|\Delta E|_{min}} = 3.45\times10^6 \frac{E_R^2 T_e}{n_e z_R^2 m_R^2}$$

Since, at most, T_e is the order of 10^{-2} keV, whereas $T_R \geq$ the order of 10 keV, the energy transfer equation reduces to the following for singly charged incident particles:

$$\frac{dE_R}{dx} = -\frac{n_e e^4 \frac{m_R}{m_e}}{8\sqrt{2\pi}\,\pi\epsilon^2 E_R \left(1+\frac{m_R kT_e}{2m_e E_R}\right)^{3/2}} \ln\left(\frac{3.45\times10^6 E_R^2 T_e}{n_e z_R^2 m_R^2}\right) \qquad \text{(C4)}$$

Ionization by Beam Ions

Ionization cross section is defined as the cross section for a collision with energy loss greater than the ionization potential U. That is,

$$Q = \int_U^{|\Delta E|_{max}} \sigma\left(|\Delta E|\right) d\left(|\Delta E|\right)$$

Substitution of equations (C1) and (C2) into this integral expression results in

$$Q_R = \frac{e^4 \frac{m_R}{m_e}}{16\pi\epsilon^2 E_R E_e}\left(\frac{v_R^2}{v_e^2 + v_R^2}\right)^{3/2}\left\{\left[-\frac{E_e}{|\Delta E|} - \frac{2}{3}\left(\frac{E_e}{\Delta E}\right)^2\right]_U^{KE_e\left(1 - \frac{v_e}{v_R}\right)}\right.$$

$$+\left[\frac{\frac{\sqrt{1 + \frac{|\Delta E|}{E_e}}}{\frac{|\Delta E|}{E_e}}\left(-\frac{1}{6} - \frac{\frac{1 + \frac{|\Delta E|}{E_e}}{3\frac{|\Delta E|}{E_e}}}{}\right) - \frac{1}{2\frac{|\Delta E|}{E_e}}\right.$$

$$\left.\left.-\frac{1}{3\left(\frac{\Delta E}{E_e}\right)^2} + \frac{1}{12}\frac{v_e}{v_R}\frac{\frac{|\Delta E|}{E_e}}{\frac{KE_R}{E_e}}\right]_{KE_R\left(1 - \frac{v_e}{v_R}\right)}^{KE_R\left(1 + \frac{v_e}{v_R}\right)}\right\} \quad \text{when} \quad U \le KE_R\left(1 - \frac{v_e}{v_R}\right)$$

$$Q_R = \frac{e^4 \frac{m_R}{m_e}}{16\pi\epsilon^2 E_R E_e}\left(\frac{v_R^2}{v_e^2 + v_R^2}\right)^{3/2}\left[\frac{\frac{\sqrt{1 + \frac{|\Delta E|}{E_e}}}{\frac{|\Delta E|}{E_e}}\left(-\frac{1}{6} - \frac{\frac{1 + \frac{|\Delta E|}{E_e}}{2E_e}}{3\frac{|\Delta E|}{E_e}}\right)\right.$$

$$\left.-\frac{1}{2\frac{|\Delta E|}{E_e}} - \frac{1}{3\left(\frac{\Delta E}{E_e}\right)^2} - \frac{1}{12}\frac{v_e}{v_R}\frac{\frac{|\Delta E|}{E_e}}{\frac{KE_R}{E_e}}\right]_U^{KE_R\left(1 + \frac{v_e}{v_R}\right)} \quad \text{when} \quad U \ge KE_R\left(1 - \frac{v_e}{v_R}\right)$$

Using $E_e = U$ for the hydrogen atoms and writing energy ratios in terms of mass and velocity ratios reduce these expressions to

$$Q_R = \frac{e^4 \frac{m_R}{m_e}}{16\pi\epsilon^2 E_R U \left(1 + \frac{v_e^2}{v_R}\right)^{3/2}} \begin{cases} \frac{5}{3} + \frac{1}{12}\left(\frac{v_e}{v_R}\right)^2 & \text{for } U \le KE_R\left(1 - \frac{v_e}{v_R}\right) \\ \frac{5}{6} + \frac{2\sqrt{2}}{3} - \frac{1}{48}\frac{v_e}{v_R}\left(\frac{v_e^2}{v_R^2} - 2\frac{v_e}{v_R} + 4\right) & \text{for } U \ge KE\left(1 - \frac{v_e}{v_R}\right) \end{cases} \tag{C5}$$

Ionization by Free Electrons

The number of ionizing encounters per unit volume per unit time between the neutral hydrogen atoms and the free electrons having a Maxwellian velocity distribution can be written as

$$n_n n_e \overline{Q_e v_e} = n_n \int Q_e v_2 f(v_2) d^3 v_2 \tag{C6}$$

where

$$f(v_2) = n_e \left(\frac{m_e}{2\pi k T_2}\right)^{3/2} \exp\left(-\frac{m_e v_2^2}{2kT_2}\right)$$

and

$$d^3 v_2 = 4\pi v_2^2 \, dv_2 \qquad \text{for spherical symmetry}$$

Since interactions are between free and bound electrons, the subscript 2 will be used temporarily for the free electrons and subscript 1 will refer to the bound electrons where demarcation is needed. There is no confusion in continuing to let n_e be the number density of free electrons and n_n the number density of neutrals, which is herein equal to the number density of bound electrons.

The preceding integration is to be made over all velocity space; however, the ionization cross section Q is zero for energy exchanges less than the ionization potential U. From equations (26) and (27) of reference 2

$$Q_e = \frac{e^4}{16\pi\epsilon^2 U^2 \left(1 + \frac{v_1^2}{v_2^2}\right)^{3/2}} \begin{cases} \frac{2}{3}\frac{E_1}{E_2} + \frac{U}{E_2}\left(1 - \frac{E_1}{E_2}\right) - \left(\frac{U}{E_2}\right)^2 & \text{when } U + E_1 \leq E_2 \\ \frac{2}{3}\left[\frac{E_1}{E_2} + \frac{U}{E_2}\left(1 - \frac{E_1}{E_2}\right) - \left(\frac{U}{E_2}\right)^2\right]\left[\left(1 + \frac{U}{E_1}\right)\left(1 - \frac{U}{E_2}\right)\right]^{1/2} & \text{when } U + E_1 \geq E_2 \geq U \end{cases}$$

This expression is for the cases wherein the mass of the target particle is equal to that of the incident particle.

Substituting the $v_2 = \sqrt{2E_2/m_e}$ and $E_1 = U$ and the last three equations into equation (C6) results in

$$\overline{Q_e v_e} = \left(\frac{m_e}{2\pi k T_e}\right)^{3/2} \frac{e^4}{2\epsilon^2 m_e^2} \left[\frac{4\sqrt{2}}{3} \int_1^2 \exp\left(-\frac{E_2}{kT_2}\right) \left(\frac{1 - \frac{U}{E_2}}{1 + \frac{U}{E_2}}\right)^{3/2} d\frac{E_2}{U} + \int_2^\infty \exp\left(-\frac{E_2}{kT_2}\right) \frac{\left(\frac{5}{3} - 2\frac{U}{E_2}\right)}{\left(1 + \frac{U}{E_2}\right)^{3/2}} d\left(\frac{E_2}{U}\right)\right]$$

Numerical evaluation of the two integrals gave the value of $\overline{Q_e v_e}$ plotted in figure 15 as a function of T_e. An empirical curve

$$\overline{Q_e v_e} = \frac{e^4}{4\pi\sqrt{2\pi m_e k T_e}\, U\epsilon^2} \left[\frac{0.0446}{e^{U/kT}}\left(1 + \frac{20.95}{e^{U/kT}}\right)\right] \tag{6}$$

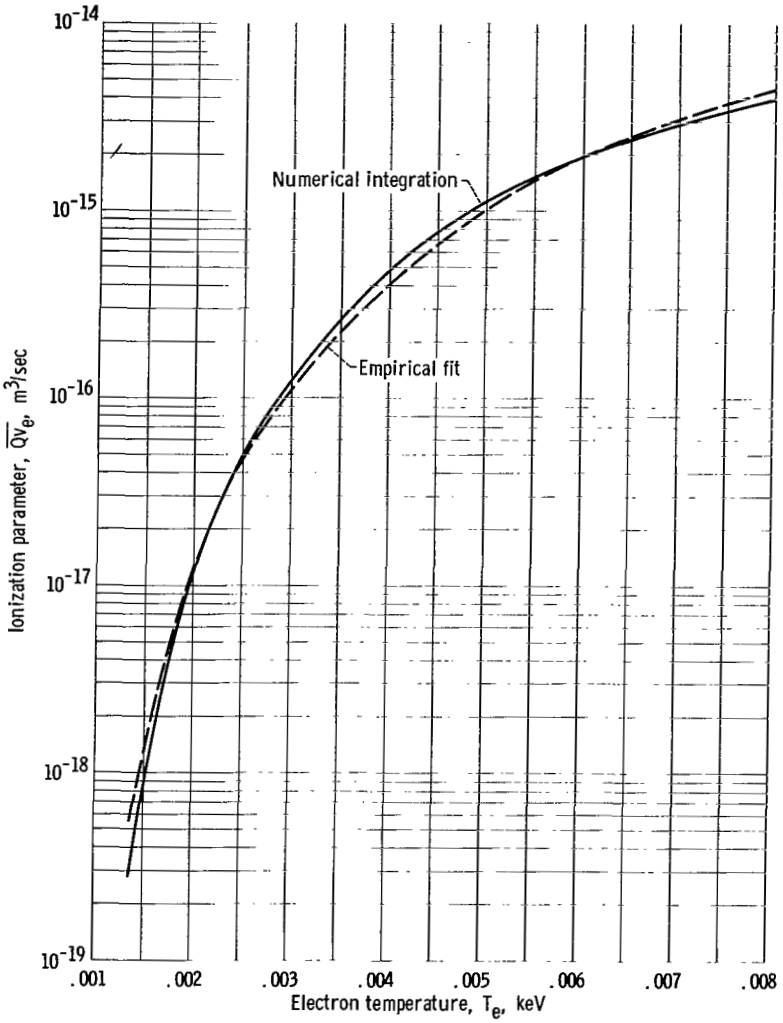

Figure 15. - Variation of ionization parameter with electron temperature.

was fitted to the numerical results. Expression (6) is shown by the dashed curve.

In an ionizing encounter all the energy given up by an incident electron, beyond that used for ionization, is given to the liberated electron in a translational mode. The liberated electron is now part of the free electron gas, and thus the net energy per unit time removed from the free electron gas is just that due to ionization, which is $Un_n n_e \overline{Q_e v_e}$. Excitation and corresponding line radiation losses can be accounted for by replacing U in this final expression by an appropriate cost per ion U'.

APPENDIX D

APPRAISAL OF ASSUMPTIONS REGARDING COLLISIONS

Numerical solution of the equations of motion over the ranges of interest now permit more detailed appraisals of some assumptions regarding collisions.

Binary Collision Assumption

Nearly all the equations developed in the preceding section are based upon the assumption of binary encounters. This approximation can be applied when the particle number densities remain below a certain limit. The reciprocal of the cube root of the number density can be used as a measure of the mean distance between neighboring particles. The most severe limitation is when Coulomb forces are involved. To obtain a characteristic length of interaction for Coulomb encounters, the author of reference 13 (p. 83) used the distance

$$r_0 = \frac{e^2}{4\pi\epsilon kT}$$

It is approximately the distance of closest approach of two mutually repelling particles. This distance is within a factor of ten of the radius of a momentum transfer cross section. For the binary collision approximation to remain valid the quantity

$$\lambda \equiv \frac{1}{r_0 n_e^{1/3}} = \frac{4\pi\epsilon kT}{e^2 n_e^{1/3}}$$

should be large.

For the range of application herein λ is at least the order of magnitude of 10 for interactions between free electrons. A plot of a typical case is shown in figure 11 (p. 27). For free electrons colliding with bound electrons, the values for λ are greater than those presented by the curve except in the very small region when $0 \leq x < 0.01$ meter. Collisions involving beam particles are not frequent enough to affect the binary collision assumption.

Thermalization of Free Electrons

The time for a distribution of electron kinetic energies to approach a Maxwellian distribution and the time between large angle deflections are given in reference 30 (p. 78) and reference 22 (p. 96). These expressions are within a factor of 1.4 of the time between the momentum transfer collisions of reference 13, which is given as

$$t_{e,e} = \frac{1}{\nu_{e,e}} = \frac{3}{8\sqrt{\pi}} \frac{\sqrt{m_e}(kT_e)^{3/2}}{\left(\frac{e^2}{4\pi\epsilon_o}\right)^2 n_e} \frac{1}{\ln\left[\frac{3}{2\sqrt{\pi}}\left(\frac{4\pi\epsilon_o kT_e}{e^2 n_e}\right)^{3/2}\right]} \tag{D1}$$

The distance for thermalization $\bar{v}_x/\nu_{e,e}$ is plotted in figure 11 for a typical set of conditions and is less than 10^{-5} meter over the most important part of the curve. The electrons should thus have ample time to thermalize.

Magnetic Force on Electrons

As discussed in the ANALYSIS section, the expression for the force that the magnetic field exerts upon the free electrons is valid if the time that the electron motion is dominated by the magnetic field is large compared with the time that the motion is collision dominated. The usual parameter for such evaluation is the ratio of cyclotron frequency to collision frequency. This parameter was most critical for collisions between free electrons for the range of variables studied herein. Equation (D1) was used to determine collision frequency $\nu_{e,e}$. A typical case is shown in figure 11 where it is seen that the magnitude of the parameter is approximately the order of 10^2.

Equilibrium of Beam

As an incident particle traverses the hydrogen target it goes through many cycles of capturing and losing an electron. The number of these cycles that occur as the energy of the particle is degraded from E_1 to E_2 is (p. 1142 of ref. 9)

$$N_c = \int_{E_1}^{E_2} \frac{\sigma_c}{\frac{1}{n_t}\frac{dE}{dx}} dE$$

where σ_c is the cross section for cycle completion. This expression provides a measure of the ability of the beam to equilibrate. The number N_c is strongly dependent on E only; thus, the conclusions of satisfactory equilibration reached in references 4 and 9, for example, should apply here also.

The number of cycles per keV of energy degradation $N_c/\Delta E$ is plotted for a typical case in figure 11. This ratio is high in the region of most importance; that is, where most of the ionization and acceleration of the propellant takes place. At a value of x of 2.5 meters, however, it falls to a value of 0.15, and then increases sharply as dE/dn approaches zero. The number of cycles per unit distance decreases from 83 at $x = 0$ to less than 1 beyond $x = 1$. In the lower cycle frequency range the assumption of an equilibrium composition is questionable. As a result, the beam may have charge compositions closer to that estimated for lower values of x. An inaccuracy would occur in the energy exchange calculation between the beam and free electrons only.

Diffusion Across Magnetic Field Lines

For a partially ionized plasma, the collisional theory coefficient of diffusion perpendicular to field lines is expressed as a constant times $\sqrt{mT}/B^2$ (ref. 22). The approximate expression for the coefficient of ambipolar diffusion across field lines is

$$\mathscr{D}_{amb} \approx \frac{2\mathscr{D}_{e_\perp}\mathscr{D}_{i_\perp}}{\mathscr{D}_{e_\perp} + \mathscr{D}_{i_\perp}}$$

The ratio of $\mathscr{D}_{amb}$ for the propellant species divided by $\mathscr{D}_{amb}$ for diffusion inside the reactor is plotted in figure 12 for one set of conditions. Since T_i is a constant in the propellant and curves of $\sqrt{T_e}$ against x have quite the same trends for all cases studied (fig. 8(c)), the curve on figure 12 is considered representative of all cases herein. In the first two mirror diameters downstream of the mirror coil, the diffusion coefficient of propellant across field lines is less than that of reactor species inside the magnetic bottle. Beyond a value of x/D of 4, however, the propellant diffusion coefficient is more than 100 times that inside the reactor. This is the region, however, where

it is desired that the propellant will cross the field lines and continue as a jet in a near axial direction.

The plasma oscillation result of Bohm (p. 462 of ref. 22) indicates that the coefficient of diffusion should be proportional to T_e/B. This would result in an even lower coefficent of diffusion in the hydrogen stream compared with that inside the reactor.

REFERENCES

1. Gryziński, Michal: Stopping Power of a Medium for Heavy, Charged Particles. Phys. Rev., vol. 107, no. 6, Sept. 15, 1957, pp. 1471-1475.

2. Gryziński, Michal: Classical Theory of Electronic and Ionic Inelastic Collisions. Phys. Rev., vol. 115, no. 2, July 15, 1959, pp. 374-383.

3. Huberman, M. N.: Partial Ionic Stopping Power and the Energy Expended in Electron Capture and Loss Collisions of Protons in Hydrogen Gas. II. Phys. Rev., vol. 127, no. 3, Aug. 1, 1962, pp. 799-804.

4. Cuevas, J.; Garcia-Munoz, M.; Torres, P.; and Allison, S. K.: Partial Atomic and Ionic Stopping Powers of Gaseous Hydrogen for Helium and Hydrogen Beams. Phys. Rev., vol. 135, no. 2A, July 20, 1964, pp. A335-A345.

5. Englert, Gerald W.: Study of Thermonuclear Propulsion Using Superconducting Magnets. Engineering Aspects of Magnetohydrodynamics, Norman W. Mather and George W. Sutton, eds., Gordon and Breach Science Publ., 1964, pp. 645-671.

6. Hilton J. L.; Luce, J. S.; and Thompson, A. S.: A Hypothetical Fusion Propulsion Rocket Vehicle. J. Spacecraft Rockets, vol. 1, no. 3, May-June 1964, pp. 276-282.

7. Rose, David J.; and Clark, Melville, Jr.: Plasmas and Controlled Fusion. MIT Press, 1961, p. 421.

8. Von Ohain, H.; Keith, B. C.; and Hunter, R. E.: Survey of Performance Potentialities of Non-Airbreathing Propulsion Systems. Vistas in Astronautics, Morton Alperin, Marvin Stern and Harold Wooster, eds., Pergamon Press, 1958, pp. 206-213.

9. Allison, Samuel K.: Experimental Results on Charge-Changing Collisions of Hydrogen and Helium Atoms and Ions at Kinetic Energies above 0.2 keV. Rev. Mod. Phys., vol. 30, no. 4, Oct. 1958, pp. 1137-1168.

10. Butler, S. T.; and Buckingham, M. J.: Energy Loss of a Fast Ion in a Plasma. Phys. Rev., vol. 126, no. 1, Apr. 1, 1962, pp. 1-4.

11. Leighten, Robert B.: Principles of Modern Physics. McGraw-Hill Book Co., Inc., 1959, pp. 494-501.

12. Evans, Robley D.: The Atomic Nucleus. McGraw Hill Book Co., Inc., 1955, pp. 575-580.

13. Burgers, J. M.: Selected Topics from the Theory of Gas Flow at High Temperatures (V). The Application of Transfer Equations to the Calculation of Diffusion, Heat Conduction, Viscosity, and Electric Conductivity. Parts I and II. Tech. Note BN-124a and b (AFOSR TN 58-427 and a), University of Maryland, May 1958.

14. Cowling, Thomas G.: Magnetohydrodynamics. Interscience Publishers, 1957, pp. 99-112.

15. Hendel, H. W.; and Reboul, T. T.: Adiabatic Acceleration of Ions by Electrons. Phys. Fluids, vol. 5, no. 3, Mar. 1962, pp. 360-362.

16. Rose, D. J.: Acceleration of a Neutralized Ion Beam. Quarterly Progr. Rep. No. 53, Massachusetts Inst. of Tech., Electronics Research Lab., Apr. 15, 1959, pp. 3-4.

17. Domitz, Stanley: Experimental Evaluation of a Direct-Current Low-Pressure Plasma Source. NASA TN D-1659, 1963.

18. Lyman, Frederic A.; Goldstein, Arthur W.; and Heighway, John E.: Effect of Seeding and Ion Slip on Electron Heating in a Magnetohydrodynamic Generator. NASA TN D-2118, 1964.

19. Brown, Sanborn C.: Basic Data of Plasma Physics. MIT Press, 1959.

20. Barnett, C. F.; Ray, J. A.; and Thompson, J. C.: Atomic and Molecular Collision Cross Sections of Interest in Controlled Thermonuclear Research. Rep. No. ORNL-3113 (Rev.), Oak Ridge National Labs., Aug. 1964.

21. Simons, J. H.; Fontana, C. M.; Muschlitz, E. E., Jr.; and Jackson, S. R.: The Low Velocity Scattering of H^+ and H_3^+ in Hydrogen. J. Chem. Phys., vol. 11, no. 7, July 1943, pp. 307-312.

22. Glasstone, Samuel; and Lovberg, Ralph H.: Controlled Thermonuclear Reactions. D. Van Nostrand Co., 1960.

23. Monnin, Carl F.; and Prok, George M.: Comparison of Gryziński's and Born's Approximations for Inelastic Scattering in Atomic Hydrogen. NASA TN D-2903, 1965.

24. Ben Daniel, D. J.: Plasma Potential in a Magnetic Mirror System. J. Nucl. Energy, Pt. C, Plasma Phys., vol. 3, no. 4, 1961, pp. 235-241.

25. Callaghan, Edmund E.; and Maslen, Stephen H.: The Magnetic Field of a Finite Solenoid. NASA TN D-465, 1960.

26. Englert, Gerald W.; and Kochendorfer, Fred D.: Estimated Performance of Radial-Flow Exit Nozzles for Air in Chemical Equilibrium. NASA Memo1-5-59E, 1959.

27. Gilbody, H. B.; and Hasted, J. B.: Ionization by Positive Ions. Roy. Soc. Proc., ser. A, vol. 240, no. 1222, June 11, 1957, pp. 382-395.

28. Fite, Wade L.; Stebbings, R. F.; Hummer, David G.; and Brackmann, R. T.: Ionization and Charge Transfer in Proton-Hydrogen Atom Collisions. Phys. Rev., vol. 119, no. 2, July 15, 1960, pp. 663-668.

29. Bauer, Ernest; and Bartky, Charlotte E.: Calculation of Inelastic Electron-Atom and Electron-Molecule Collision Cross Sections by Classical Methods. Publ. No. U-2943, Philco Corp. Aeronutronic Div., Jan. 1965. (Available from DDC as AD627033.)

30. Spitzer, Lyman: Physics of Fully Ionized Gases. Interscience Publishers, Inc., 1956.

"The aeronautical and space activities of the United States shall be conducted so as to contribute . . . to the expansion of human knowledge of phenomena in the atmosphere and space. The Administration shall provide for the widest practicable and appropriate dissemination of information concerning its activities and the results thereof."

—NATIONAL AERONAUTICS AND SPACE ACT OF 1958

NASA SCIENTIFIC AND TECHNICAL PUBLICATIONS

TECHNICAL REPORTS: Scientific and technical information considered important, complete, and a lasting contribution to existing knowledge.

TECHNICAL NOTES: Information less broad in scope but nevertheless of importance as a contribution to existing knowledge.

TECHNICAL MEMORANDUMS: Information receiving limited distribution because of preliminary data, security classification, or other reasons.

CONTRACTOR REPORTS: Technical information generated in connection with a NASA contract or grant and released under NASA auspices.

TECHNICAL TRANSLATIONS: Information published in a foreign language considered to merit NASA distribution in English.

TECHNICAL REPRINTS: Information derived from NASA activities and initially published in the form of journal articles.

SPECIAL PUBLICATIONS: Information derived from or of value to NASA activities but not necessarily reporting the results of individual NASA-programmed scientific efforts. Publications include conference proceedings, monographs, data compilations, handbooks, sourcebooks, and special bibliographies.

Details on the availability of these publications may be obtained from:

SCIENTIFIC AND TECHNICAL INFORMATION DIVISION

NATIONAL AERONAUTICS AND SPACE ADMINISTRATION

Washington, D.C. 20546